

## GIANT RADIO QUASARS: SAMPLE AND BASIC PROPERTIES

AGNIESZKA KUŹMICZ<sup>1,2</sup> AND MAREK JAMROZY<sup>1</sup>

<sup>1</sup>*Astronomical Observatory, Jagiellonian University, ul. Orła 171, 30-244 Krakow, Poland*

<sup>2</sup>*Queen Jadwiga Astronomical Observatory in Rzepiennik Biskupi, 33-163 Rzepiennik Strzyżewski, Poland*

(Received July 1, 2016; Revised September 27, 2016; Accepted December 17, 2020)

Submitted to ApJS

### ABSTRACT

We present the largest sample of giant radio quasars (GRQs), which are defined as having a projected linear size greater than 0.7 Mpc. The sample consists of 272 GRQs, of which 174 are new objects discovered through cross-matching the NRAO VLA Sky Survey (NVSS) and the Sloan Digital Sky Survey 14<sup>th</sup> Data Release Quasar Catalogue (DR14Q) and confirmed using Faint Images of the Radio Sky at Twenty-Centimeters (FIRST) radio maps. In our analysis we compare the GRQs with 367 smaller, lobe-dominated radio quasars found using our search method, as well as with quasars from the SDSS DR14 Quasar Catalogue, investigating the parameters characterizing their radio emission (i.e. total and core radio luminosity, radio core prominence), optical properties (black hole masses, accretion rates, distribution in Eigenvector 1 plane) and infrared colours. For the GRQs and smaller radio quasars we find a strong correlation between [OIII] luminosity and radio luminosity at 1.4 GHz, indicating a strong connection between radio emission and conditions in the narrow-line region. We spot no significant differences between GRQs and smaller radio quasars, however we show that most extended radio quasars belong to a quasar population of evolved AGNs with large black hole masses and low accretion rates. We also show that GRQs have bluer W2-W3 colours compared to SDSS quasars with FIRST detections, indicating differences in the structure of the dusty torus.

*Keywords:* galaxies: active – galaxies: nuclei – galaxies: structure

arXiv:2012.08857v1 [astro-ph.GA] 16 Dec 2020

## 1. INTRODUCTION

Giant radio sources (GRSs) are objects with extremely large projected linear sizes ( $> 0.7$  Mpc; assuming  $H_0=71$  km s<sup>-1</sup>Mpc<sup>-1</sup>,  $\Omega_M=0.27$ ,  $\Omega_\Lambda=0.73$ ; Spergel et al. 2019). It is believed that such large radio size structures are relatively rare. Only  $\sim 6\%$  of radio sources from the 3CR complete sample do exceed this size (e.g. Ishwara-Chandra & Saikia 1999). The reasons why some radio sources have grown so large are not fully understood, however detailed multi-wavelength studies have significantly increased our knowledge about the nature of GRSs (e.g. Jamrozy et al. 2008, Machalski, Jamrozy & Saikia 2009, Konar et al. 2008, Kuligowska et al. 2009, Subrahmanyan et al. 2008).

The crucial point in research of the GRS' origin is to study large and homogeneous samples of such objects. Owing to the efforts of many scientists, a lot of new GRSs were found during the last several years. Kuźmicz et al. (2018) catalogued all the GRSs found in the literature up to 2018. The sample includes 349 GRSs, of which 280 are hosted by galaxies (giant radio galaxies; GRGs) and 69 by quasars (giant radio quasars; GRQs). The second-largest sample of GRSs was compiled by Dabhade et al. (2020a). Based on the low-frequency LOFAR Two-metre Sky Survey first data release (LoTSS; Shimwell et al. 2017, 2019), the authors collected 239 GRSs (199 GRGs and 40 GRQs). This release covers a region of only 424 deg<sup>2</sup>, but the LOFAR survey is very sensitive to low surface brightness features and has a high angular resolution, which makes it a valuable tool in identifying extended radio galaxies. A smaller sample of GRSs was also compiled by Kozieł-Wierzbowska et al. (2020), as part of the ROGUE project within which the authors catalogued 33 GRGs. Recently, a new large catalogue is being prepared by Dabhade et al. (2020b) under the SAGAN project, where authors collected 162 GRSs (139 GRGs and 23 GRQs) using NVSS (Condon et al. 1998), FIRST (Becker, White & Helfand 1995), and the TIFR GMRT Sky Survey (TGSS; Intema et al. 2017). In total, we know at least about 770 GRSs, of which only 109 are considered as GRQs. In the 3CRR complete sample of radio sources with flux density limit 10 Jy (Laing et al. 1983), 75% of radio sources are radio galaxies, and 25% are radio quasars, according to the NASA Extragalactic Database (NED, ned.ipac.caltech.edu). The smaller fraction of GRQs in the entire GRS population indicates that selection effects play a significant role in their identification.

The connection between the production of powerful jets and the conditions within the innermost regions of active galactic nuclei (AGN) has not been fully explored. Various studies have attempted to understand the phys-

ical processes underlying the optical and radio emission in quasars (e.g. Jackson & Browne 1991, Willott et al. 1999, Miller et al. 1999, Sulentic et al. 2002, Kimball et al. 2011, Jackson & Browne 2013, Olmo et al. 2020, Gaur et al. 2019). A lot of research has concentrated on testing unified schemes where radio-loud quasars are supposedly galaxies with a central supermassive black hole (BH) surrounded by an accretion disk, a dusty torus and clouds of gas. They can generate powerful radio jets directed along the rotation axis of the BH. The anisotropic emission due to torus obscuration as well as relativistic boosting of radio jet emission leads to the orientation effects visible in optical and radio bands. Certain spectral parameters were found to correlate with the radio source's orientation. For example, Kharb & Shastri (2004) found a correlation between nuclear optical luminosity and radio core prominence, which can be used as an orientation indicator. Also, the equivalent widths of broad emission lines are found to be orientation-dependent e.g. Baker (1997) and Kimball et al. (2011), although the authors obtained contradictory results claiming respectively anticorrelation and correlation between those two parameters. However, the basic AGN model predicts a stronger continuum emission in sources viewed closer to the radio-jet axis, which leads to smaller values of equivalent widths.

The connection between the extended radio luminosity and luminosities of narrow emission lines found by different authors (e.g. Baum & Heckman 1989, Rawlings et al. 1989, Tadhunter et al. 1998, Gaur et al. 2019) indicates that the source responsible for narrow-line emission is actually also the source of radio emission (Rawlings & Saunders 1991), in contrast to other models in which radio and narrow-line luminosities are mainly driven by the environment (Dunlop & Peacock 1993). The narrow-line and radio emission are most likely related to the accretion rate and/or the BH mass, which are also drivers of AGN evolution.

The GRSs that are supposed to be sources in an advanced evolutionary stage, were studied in terms of their optical properties by Kuźmicz & Jamrozy (2012). The authors analysed BH masses, accretion rates, and radio properties for a sample of 45 GRQs. As a result, they discovered that GRQs are very similar to smaller radio quasars and the determined parameters are typical for powerful quasars. It has to be noted that the analysed sample was relatively small as compared to the number of GRQs known to date. Therefore, we decided to re-examine optical properties of GRQs, focusing on various aspects which had not been explored yet.

The aim of this work is to complement the existing samples of GRSs with new objects which are hosted by

quasars. While the number of known GRGs ( $\sim 650$ ) is relatively high, the GRQs constitute only  $\sim 14\%$  of all known GRGs. It is much less than in the 3CRR sample where the QSOs constitute 25% of radio sources. It has to be emphasized that our sample enlarges the number of known GRQs nearly threefold, which shows our method to be an efficient way of finding GRGs. The second part of this study concentrates on some fundamental properties observed in AGNs, i.e. the quasar main sequence, infrared colour diagram, and radio core prominence. We compare properties of GRQs with smaller-sized extended radio quasars (SRQs), as well as with the SDSS quasars that have matches with a FIRST radio source according to the SDSS data release 14 Quasar catalogue (DR14Q; Pâris et al. 2018) to look for differences between the GRQs and other quasars.

## 2. SAMPLE SELECTION

For our analysis, we collected GRQs known to date, along with 174 new objects, which makes our sample the largest one containing such a rare class of radio sources. 69 GRQs out of all previously known GRQs were taken from the literature compilation of GRGs by Kuźmicz et al. (2018). A further 15 GRQs were taken from Dabhade et al. (2020a), where authors identified them on low frequency radio images of the LoTSS survey, and another 14 GRQs were taken from Dabhade et al. (2020b). The new GRQs studied in this paper were found using the currently available data from the NVSS, FIRST and DR14Q catalogues. These catalogues were already used in a systematic search of GRGs (e.g. Proctor (2016), Dabhade et al. (2017), Dabhade et al. (2020b)). However, e.g. Proctor (2016) selected only radio sources with angular size larger than  $4'$ . In our study we do not apply any restriction on angular size and we found 59 new GRQs with angular sizes larger than  $4'$ . Therefore, in order to find extended radio sources, future search methods have to be improved.

The combined sample of new and known GRQs comprises 272 objects, which significantly enlarges the number of known GRQs. The newly discovered 174 GRQs and their basic parameters are listed in Table 1.

### 2.1. GRQ search method

In searching extended radio quasars we used the DR14Q quasar catalogue, including 526 356 spectroscopically identified quasars and quasar candidates. All of the catalogued quasars were cross-matched with the NVSS radio sources in the following way:

- In the first step, using the DS9 software<sup>1</sup> we plotted the positions of all quasars from the DR14Q on the full NVSS atlas images of  $4^\circ \times 4^\circ$  in size. Only  $\sim 1000$  NVSS images had DR14Q objects in them and typically each NVSS image had about 500 such quasars. Around each quasar position we drew a circle corresponding to the expected 0.7 Mpc angular size, considering the redshift of each quasar.
- In the second step we visually inspected all the full NVSS atlas images containing DR14Q objects, looking for radio sources exceeding the size of the plotted circles. We considered only the sources where the quasar position was near the centre of radio emission i.e. in a centre of single apparent elongated emission, between two maxima of radio emission, or in a maximum of radio emission between two nearly symmetrically located maxima. Due to such a selection strategy we could have missed very asymmetric radio sources and sources with a one-sided radio lobe visible in NVSS maps. As a result we selected 1341 quasars with visible elongated NVSS radio emission exceeding 0.7 Mpc in size.
- In the next step we manually verified all positive matches using FIRST and AllWISE infrared images (Cutri et al. 2013) and SDSS optical images to discern false findings. We visually inspected whether radio hot-spots coincide with optical or infrared sources. We also checked if the positions of optical quasar hosts coincide with the FIRST radio core emissions. Almost all the quasars from our sample have radio cores in the FIRST survey catalogue separated by less than  $1''$  from the optical quasar. We confirmed that 603 out of 1341 selected quasars are the hosts of extended radio sources. Based on the FIRST radio maps, we measured the projected linear size (distance between the opposite hot-spots) of GRQ candidates. As a result, a lot of radio quasars proved to be actually smaller than 0.7 Mpc, despite their projected linear size on the NVSS maps (as measured to the  $3\sigma$  contour level – step two of the search method) exceeding 0.7 Mpc (Section 2.2). In some cases the difference between both these methods of radio source size measurement, from one hot-spot to opposite hot-spot on the FIRST maps and from  $3\sigma$  contour level of one lobe to  $3\sigma$  contour level of the

<sup>1</sup> <http://ds9.si.edu>

opposite lobe on the NVSS maps, is very large. This can be particularly well seen in the case of high-redshift quasars that have small angular sizes (e.g. for redshift  $z=1$  the NVSS beam size equal to  $45''$  corresponds to  $\sim 360$  kpc), for which NVSS  $3\sigma$  sizes are overestimated more than twofold. Therefore, in our study we use radio source size measurements from the hot-spot to hot-spot method on the FIRST maps, while NVSS  $3\sigma$  sizes were used only in the process of GRQs candidates selection. The difference between the two methods of radio source size measurement is illustrated in Figure 1. For the radio sources with no radio core emission detected in the FIRST survey, we checked the host position using the Very Large Array Sky Survey (VLASS; Lacy et al. 2020) all-sky radio survey at 3 GHz with high angular resolution ( $\sim 2.''5$ ). We also used VLASS maps to determine angular sizes of radio sources which are outside the FIRST survey footprint or have FIRST radio structure visible only on one side of the host quasar. They are marked with letter “v” in Tables 1 and 2. In the cases where there was no possibility to measure the radio source’s size from hot-spot to hot-spot (because there were no FIRST or VLASS detections), we give an approximated value measured between NVSS maxima of lobe emission (marked as “m” in Tables 1 and 2) or between the FIRST hot-spot and the NVSS maximum on the opposite side in the case of one-sided FIRST radio lobes (marked as “fn” in Tables 1 and 2). In our study we use only the radio source size measurements listed in Tables 1 and 2.

It is worth to highlight that using the method described above we “re-discovered” almost all the GRQs from Kuźmicz et al. (2018) within the field of the NVSS/SDSS surveys. Moreover, we found 15 out of 40 GRQs which have been found earlier by Dabhade et al. (2020a) based on the low-frequency LoTSS radio maps. A further 19 GRQs from Dabhade et al. (2020a) are too small to meet the GRS size criterion, based on measurements of their radio structures on FIRST maps, therefore we do not include them in the sample of known GRQs. Of the 23 new GRQs found by Dabhade et al. (2020b), 6 GRQs were identified also in our search method, and 11 occurred to have hot-spot to hot-spot FIRST sizes smaller than 0.7 Mpc. These 11 QSOs were also not included in the sample of known GRQs. It has to be noted here that in Dabhade et al. (2020a) the authors measured sizes of radio sources up to the  $3\sigma$  level on low resolution ( $20''$ ) LOFAR maps, and in Dabhade et al. (2020b) up to the  $3\sigma$  level on NVSS maps, there-

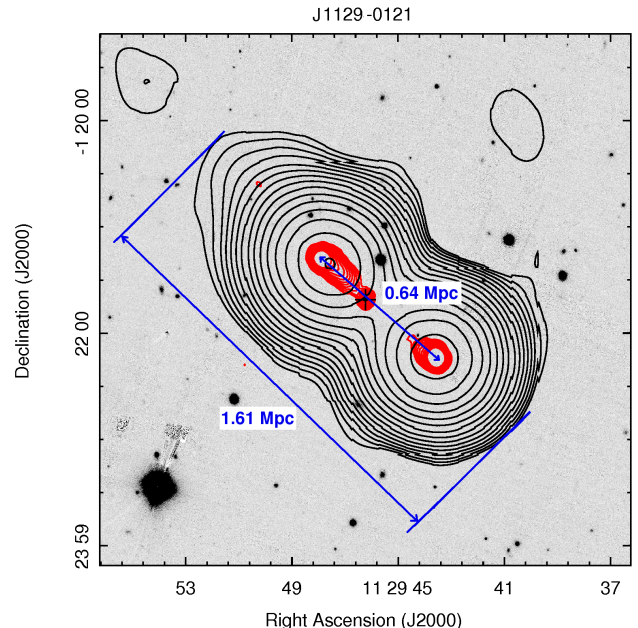


**Figure 1.** The GRQ J1129-0121 located at  $z=0.726$ . The NVSS black contours and FIRST red contours are overlaid on an r-band Pan-STARRS optical image. The Figure shows the difference between radio source size measurement methods. In Dabhade et al. (2020b) J1129-0121 is measured to  $3\sigma$  NVSS contour level giving the largest linear size  $D=1.61$  Mpc. The measurement from FIRST hot-spot to hot-spot results the  $D=0.64$  Mpc, disqualifying this quasar as a GRQ. In our study the J1129-0121 is classified as SRQ.

fore their results are overestimated. In our study, for the quasars taken from Dabhade et al. (2020a) and Dabhade et al. (2020b) we use remeasured sizes from hot-spot to hot-spot on FIRST maps.

## 2.2. Subsample of smaller radio quasars

The method described above allowed for identification of extended radio quasars with NVSS  $3\sigma$  sizes larger than 0.7 Mpc. As was mentioned in Section 2.1, some of the radio quasars selected in the second step of the search method proved to be smaller than 0.7 Mpc after remeasuring their sizes from hot-spot to hot-spot in the FIRST radio maps. In our study such quasars are classified as SRQs.

In the SRQ sample we collected 367 objects that we found using our search method. They are listed in Table 2. Their projected linear sizes are between 0.2 – 0.7 Mpc, so they are not GRQs but represent the population of extended radio quasars which can be used in other studies. Together with GRQs they provide a sample covering a continuous size range of smaller and larger radio quasars. The number of quasars in SRQ sample (with  $3\sigma$  sizes larger than 0.7 Mpc and hot-spot to hot-spot sizes smaller than 0.7 Mpc) shows that in samples



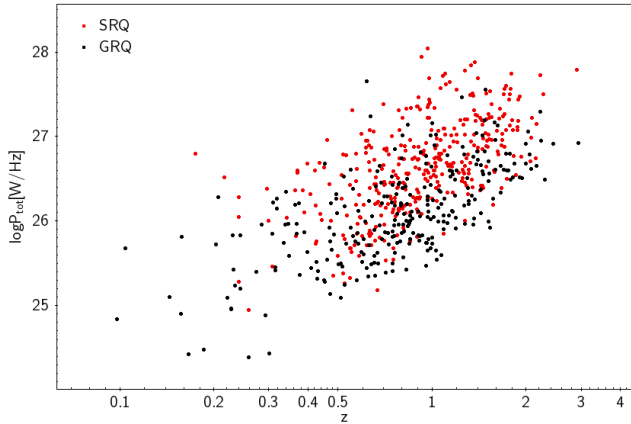


**Figure 2.** The total radio luminosity at 1.4 GHz as a function of redshift for the GRQ (black dots) and SRQ (red dots) samples.

where the  $3\sigma$  method is used for size measurement, radio source sizes can be even triply overestimated.

### 2.3. Characteristics of the sample

The characteristic parameters of the GRQ (174 new findings and 98 previously known GRQs listed in [Kuźmicz et al. 2018](#), [Dabhade et al. 2020a](#) and [Dabhade et al. 2020b](#)) and SRQ samples are presented in Figure 2 and 3, where we plot the redshift versus 1.4 GHz total radio luminosity ( $P_{\text{tot}}$ ) and total radio luminosity – linear size diagram, respectively. The  $P_{\text{tot}}$  for newly identified GRQs and SRQs was determined by applying the formula given by [Brown, Webster & Boyle \(2001\)](#), where we used the 1.4 GHz flux-densities measured on the NVSS maps, adopting the spectral index value  $\alpha = -0.6$  (after [Wardle & Aaron 1998](#)). We use the convention of  $S_\nu \sim \nu^\alpha$ . In order to estimate the core radio luminosity ( $P_{\text{core}}$ ) analysed in the next sections, we measured core flux densities on the FIRST maps and used  $\alpha = -0.3$  from [Zhang et al. \(2003\)](#).

The quasars from our samples cover the redshift range of  $0.1 < z < 3$  and the median value of projected linear size ( $D$ ) for GRQs is  $D=0.9$  Mpc and for SRQs  $D=0.44$  Mpc. The median value of 1.4 GHz total radio luminosity is  $\log P_{\text{tot}} [\text{WHz}^{-1}] = 26.1$  for the GRQ sample and  $\log P_{\text{tot}} [\text{WHz}^{-1}] = 26.6$  for the SRQ sample. The smaller median value of  $P_{\text{tot}}$  for GRQs is in agreement with existing radio source evolutionary models (e.g. [Kaiser et al. 1997](#)), where the larger radio sources are older and thus have lower total radio luminosities. It can be clearly seen in Figure 3, where we plotted  $P_{\text{tot}}$  against the projected linear size measured from hot-spot to hot-spot (column 6 in Table 1), that  $P_{\text{tot}}$  decreases as the projected linear size increases. The distributions of  $P_{\text{tot}}$  and  $D$  for both the samples are presented in Figure 4.

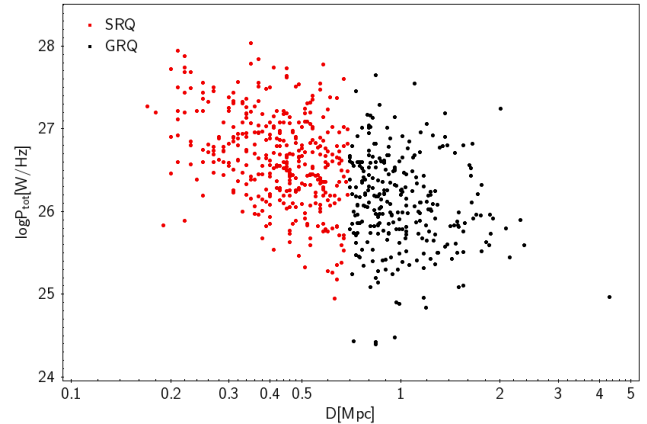


**Figure 3.** Luminosity – linear size diagram for GRQs and SRQs. The symbols are the same as in Figure 2. In the figure we use the linear size measured as the distance between hot-spots.

The largest GRQ J0931+3204 measures 4.29 Mpc ([Coziol et al. 2017](#)).

In Figure 5, we plot the distribution in redshift for our samples in comparison with the distribution for GRGs hosted by galaxies. It can be seen that the highest number of GRQs and SRQs is at the redshift  $z \sim 0.8$ , while for GRGs the maximum of distribution is at  $z=0.2$ . The differences in redshift distributions for GRQs and GRGs are caused by selection effects. The galaxies at higher redshifts are hard to observe, while the highest number of SDSS DR14 quasars is observed at  $z \sim 1.5$  and  $z \sim 2.2$  with only  $\sim 50$  objects below  $z=0.1$ .

- High redshift ( $z > 1$ ) GRGs are very rare because the IGM density is higher at earlier cosmological epochs and also because the surface brightness of the radio structure strongly depends on redshift, which makes them hard to be detected and identified. Until now, 31 GRQs at  $z > 1$  of which only 6 have  $z > 2$  had been reported in literature ([Kuźmicz et al. 2018](#); [Kuligowska & Kuźmicz 2018](#); [Dabhade et al. 2020a](#)). In the presented sample of GRQs, there are 70 new QSOs at  $z > 1$ , of which 9 are located at  $z \geq 2$ . This significantly increases the number of known high-redshift GRGs. The radio maps of the most distant newly discovered GRQs are presented in Figure 6, where we plotted NVSS and FIRST or VLASS contours overlaid onto r-band Pan-STARRS ([Flewelling et al. 2020](#)) optical image. The most distant GRQ is J1411+0156 located at  $z=2.95$ . As can be seen on the radio map of J1411+0156, there is no radio bridge connecting the radio core and the western radio lobe. Moreover, there is a very faint infrared object in the unWISE Catalog ([Schlafly et al. 2019](#)) which

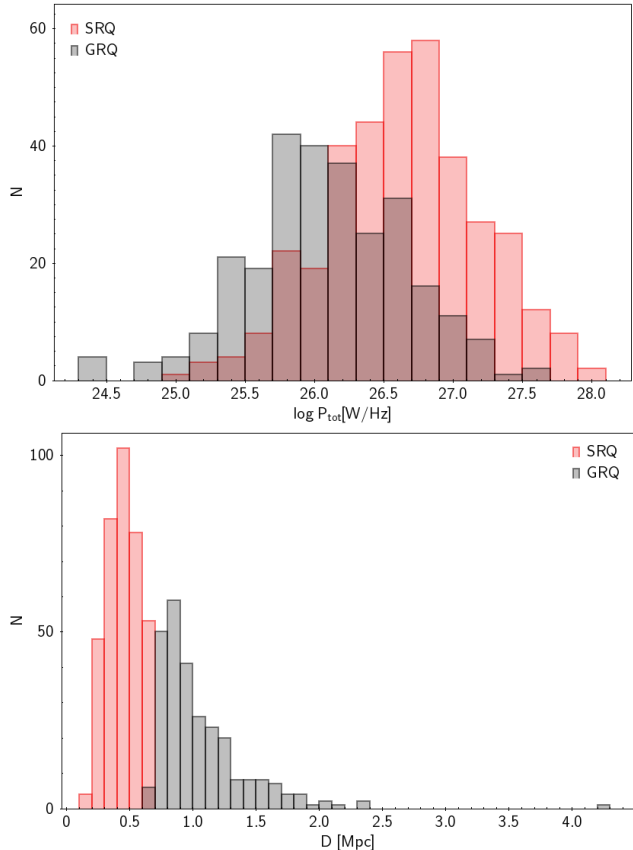


**Figure 4.** Distribution of  $P_{\text{tot}}$  (top panel) and  $D$  (bottom panel) for GRQ and SRQ samples.

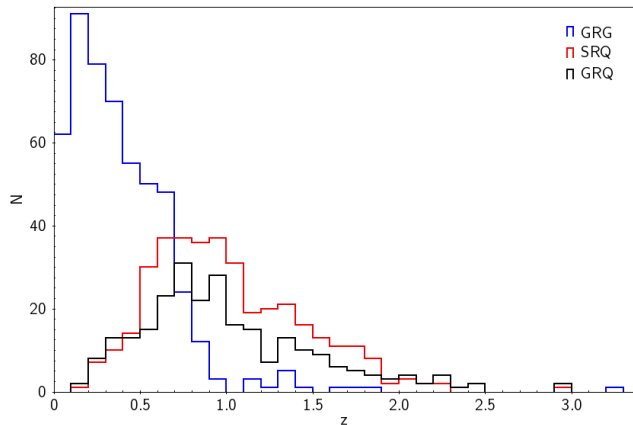


**Figure 5.** Distribution of redshift for GRQs (black line), SRQs (red line) and GRGs (blue line).

coincides with the western radio lobe. Therefore better sensitivity radio data are needed to full confirmation this radio quasar as a GRQ.

- X-ray detections. It is expected that for more distant sources the X-ray-to-radio flux ratio increases due to higher energy density of the cosmic

microwave background (CMB). At higher redshift the relativistic electrons in radio jets preferentially lose energy due to scattering on CMB photons (e.g. Simionescu et al. 2016, Ghisellini et al. 2014). For quasars included in our samples 72 (of the 174) GRQs and 96 (of the 367) SRQs have detections in the ROSAT all-sky survey (Voges et al. 2000, 1999), while 10 GRQs and 18 SRQs are listed in the Third XMM-Newton Serendipitous Source Catalog (Rosen et al. 2016). The most distant GRQs from our sample have not been detected in X-rays to date, so they constitute good targets for future X-ray observations.

#### 2.4. One-sided radio jets

Some quasars from our samples show evidence of a one-sided radio jet visible very close to the host quasar. In the samples of GRQs and SRQs we found 7 and 26 such quasars, respectively. The presence of one-sided radio jets indicates the Doppler boosting of radio emission due to high radio source inclination of radio jets. Therefore, the projected sizes of such radio sources may be highly underestimated. The quasars with visible one-sided radio jet are marked with letter “j” in Tables 1 and 2.

### 3. RADIO CORE PROMINENCE PARAMETER

For the quasars from our samples, we determined the radio core prominence parameter ( $f_c$ ) defined as the ratio between the core flux density ( $S_{\text{core}}$ ) and the extended radio emission flux density ( $S_{\text{ext}} = S_{\text{tot}} - S_{\text{core}}$ ),  $f_c = S_{\text{core}}/S_{\text{ext}}$ , (named as R parameter in Orr & Browne 1982). It was postulated by many authors that  $f_c$  is a good indicator of radio source orientation. A high value of the  $f_c$  parameter indicates that the radio source jets are oriented closer to the line of sight. The dependence of optical properties on the  $f_c$  parameter can result from relativistically beamed radiation or anisotropically emitted radiation due to obscuration in some directions or a line-emitting region which is not spherically symmetric (Jackson & Browne 1991), therefore it can be used to probe the structure of central regions in AGNs.

In our study, the  $f_c$  parameter was estimated only for those radio quasars for which we were able to separate the radio core from the extended radio emission. We did not use quasars with no radio core detection in FIRST catalogue. The radio core flux density was measured on FIRST radio maps, which have a better resolution than NVSS, while the total flux densities were measured on NVSS maps to avoid losing weak and diffuse radio emission of radio lobes. In the sample of GRQs we determined  $f_c$  for 225 GRQs, of which 18 have  $f_c > 1$ . An

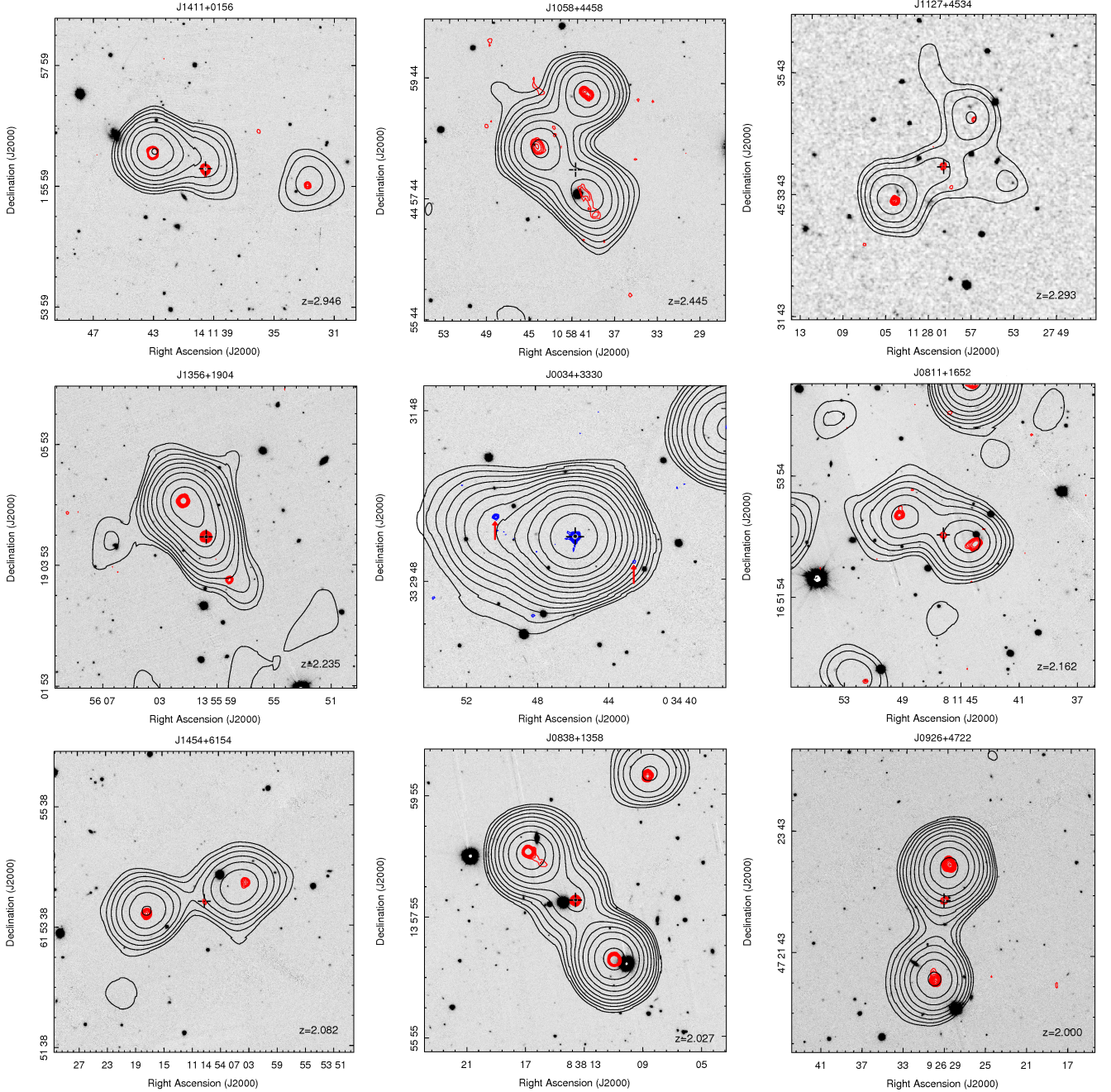


**Figure 6.** Radio maps of new GRQs located at  $z \geq 2$ . The NVSS black contours are overlaid onto r-band Pan-STARRS optical images. The FIRST radio contours are plotted in red and the VLASS contours in blue. The cross marks the position of the parent QSO and the red arrows in the J0034+3301 image mark the position of VLASS hot-spots

$f_c$  value larger than one means that the radio core dominates the overall luminosity of the radio source. In the sample of SRQs we measured  $f_c$  for 284 quasars, of which only 6 have  $f_c > 1$ .

We checked the correlations between the radio core dominance and equivalent widths (EWs) of different emission lines. The measurements of emission lines were done by Rakshit et al. (2020), where the authors es-

timate spectral parameters for all quasars in DR14Q. It was predicted by different models that the emission line properties depend on orientation. Such a dependence can be caused by obscuration by a clumpy torus, Doppler-boosting of continuum emission or inclination of the accretion disk (Nenkova et al. 2008, Browne & Murphy 1987, Netzer 1987). We obtained the strongest correlation between  $\log \text{EW}(\text{H}\alpha)$  and  $\log f_c$  (the corre-



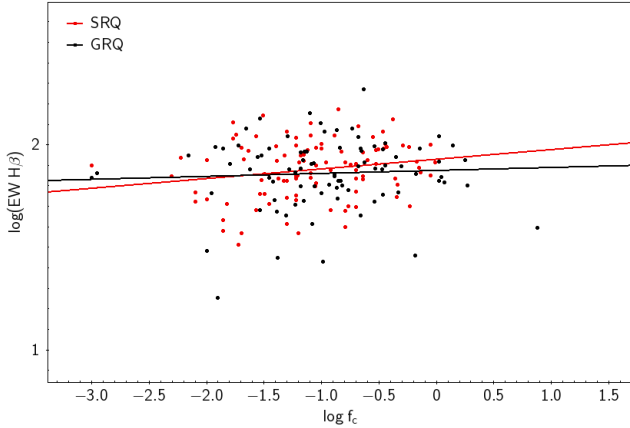


**Figure 7.** The equivalent width of the  $H\beta$  line versus the radio core prominence parameter  $f_c$ . The fitted lines were obtained via the standard linear regression model. The same method was applied in Figures 8, 9 and 10.

lation coefficient of linear fit ( $C$ ) is  $C=0.57$  for GRQs and  $C=0.49$  for SRQs), but it should be noted that we found the  $H\alpha$  line to be present in the spectra of only a few quasars, so this result is not representative for the entire sample. The EW of  $H\beta$  broad emission line is very weakly correlated with  $f_c$  ( $C=0.06$  for GRQs and  $C=0.19$  for SRQs), however the overall trend of increasing  $EW(H\beta)$  with  $f_c$  can be seen (Figure 7). Also other broad emission lines, like  $H\gamma$ ,  $MgII$  and  $CIV$ , are very weakly correlated with  $f_c$ . In AGN models, it was predicted that the broad emission lines, which are produced close to the accretion disk, should be orientation-dependent and emitted anisotropically (e.g. Jackson & Browne 1991). The lack of correlation between broad emission lines and  $f_c$  parameter indicates that EW does not depend on orientation or that both the emission line and optical continuum show the same dependence on orientation. On the other hand, the  $f_c$  parameter may be not a good indicator of orientation for very extended radio sources because the aged radio lobes will have significantly decreased surface brightness due to radiation losses and adiabatic expansion. Also jet interactions with the intergalactic medium, as well as cosmological surface brightness dimming may affect the observed flux of extended radio structures in GRQs. It is also possible that in the case of quasars with a very high  $f_c$ , the high core flux density can be caused by recurrent radio jet emission, which cannot be resolved in too low resolution radio maps (e.g. 4C +02.27, Kuźmicz et al. 2017).

For our samples of quasars, we do not find either the strong anticorrelation between EW of [OIII] and  $f_c$  (Figure 8) observed by other authors (Baker 1997, Jackson et al. 1989, Jackson & Browne 2013). The anticorrelation is predicted by the model in which the broad line region

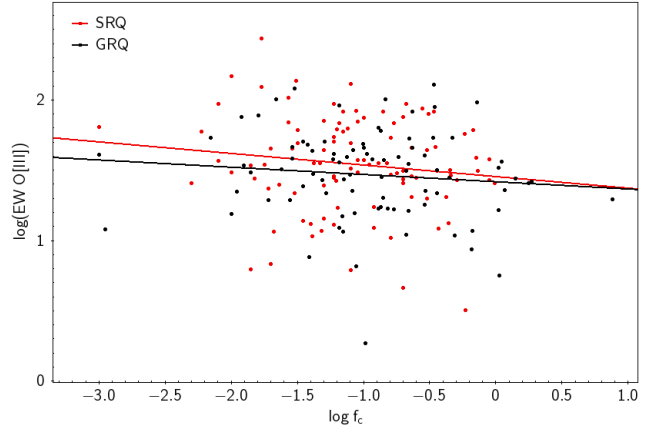


**Figure 8.** The equivalent width of the [OIII] line against  $f_c$  parameter.

(BLR) is photo-ionized by radiation from the accretion disk and the strength of emission lines is correlated with the intensity of this radiation. When our line of sight is near perpendicular to the plane of the obscuring torus of the AGN (high  $f_c$ ), a low EW of [OIII] is expected. For larger inclinations (smaller  $f_c$ ), a higher EW should be observed due to obscuration of the ionizing component. The very weak anticorrelation for our GRQs and SRQs ( $C\sim-0.12$ ) may have resulted from a small number of core-dominated quasars in our samples and because the  $f_c$  parameter may be not a good indicator of radio source orientation. Another possibility is that for very extended radio quasars, the structure of innermost parts of AGN (the dusty torus) does not lead to anisotropic obscuration of the ionizing continuum source.

#### 4. [OIII] LUMINOSITY - RADIO LUMINOSITY RELATION

For our samples of QSOs, we checked the relation between [OIII] luminosity ( $L[OIII]$  values are taken from Rakshit et al. 2020) and total radio luminosity  $P_{tot}$ , as well as the core radio luminosity  $P_{core}$  at 1.4 GHz (Figure 9 and 10), which indicates a possible connection of radio jet emission with the narrow line region (NLR). For the sample of GRQs we obtained a relatively high level of correlation. For the  $L[OIII]$  vs  $P_{tot}$  relation, the correlation coefficient  $C$  is 0.71 and for  $L[OIII]$  vs.  $P_{core}$   $C=0.57$ . A lower, but still high level of correlation, was found in the sample of SRQs. The correlation coefficients of the  $L[OIII]$  vs.  $P_{tot}$  and  $L[OIII]$  vs.  $P_{core}$  relations are  $C=0.61$  and  $C=0.53$  respectively. Also, when we consider the relation between  $L[OIII]$  and radio luminosity of extended radio emission ( $P_{ext}=P_{tot}-P_{core}$ ), there are considerable correlations in both the samples, much stronger than those obtained by Gaur et al. (2019) for a sample of radio-loud quasars ( $C=0.25$ ) or by Tad-



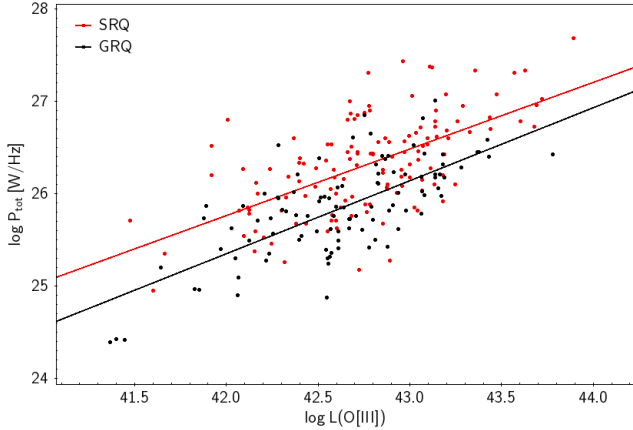


**Figure 9.** Relation of the total radio luminosity at 1.4 GHz and the luminosity of [O III].

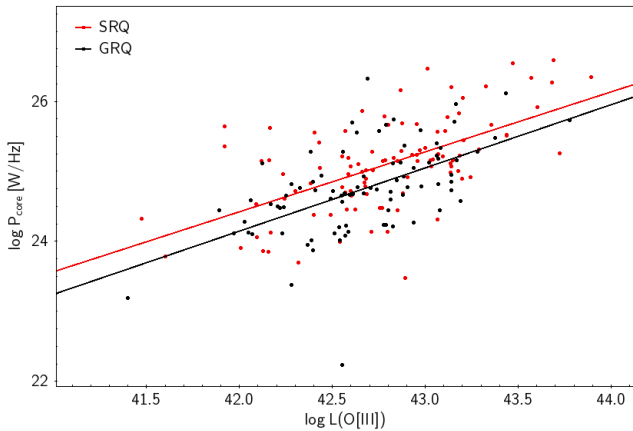


**Figure 10.** Relation of the core radio luminosity at 1.4 GHz and the luminosity of [O III].

hunter et al. (1998) for the 2 Jy complete sample of radio sources ( $C=0.38$ ). It may indicate that the connection between radio emission and the NLR in GRQs is quite significant. In the standard quasar illumination model (e.g. Rawlings & Saunders 1991) the correlation between radio and [OIII] luminosity is explained as due to a direct relation between the power of the photoionizing continuum and the radio jet power.

## 5. EIGENVECTOR 1

A powerful tool for probing AGN properties and the fundamental correlations between different spectral components is Eigenvector 1 (EV1; Boroson & Green 1992). The EV1 optical plane is defined by the FWHM of the broad  $H\beta$  line and the ratio  $R_{FeII}$  between the EW of FeII (4435–4685Å) and the EW of the  $H\beta$  broad line. The location of an object in the plane of EV1 traces the so-called quasar main sequence. In the EV1 plane two different spectral types of QSOs can be distinguished:

population A with  $FWHM H\beta \leq 4000$  km/s and population B with  $FWHM H\beta > 4000$  km/s. Sources which belong to the same spectral type have similar spectroscopic properties, e.g. line flux ratios and line profiles (Sulentic et al. 2002). The  $R_{FeII}$  parameter traces the variation of Eddington ratio  $L/L_{Edd}$ , while the FWHM of  $H\beta$  traces a change in orientation (Marziani et al. 2001, Sulentic et al. 2017). It was postulated by Zamfir & Fan (2008) and Marziani et al. (2018) that the separation line between populations A and B at  $FWHM H\beta=4000$  km/s can correspond to a critical change in accretion disk structures: from wind-dominated geometrically thick accretion disk in population A to the geometrically thin disk-dominated population B.

In Figure 11, we plotted the EV1 plane for GRQs and SRQ samples. All the spectral parameters used in this study were taken from Rakshit et al. (2020). In Figure 11, we also plotted the location of all 18 273 quasars which are flagged in DR14Q as quasars with FIRST counterparts within  $2''$  (Pâris et al. 2018). We refer to this sample as the DR14Q FIRST quasars. In drawing the diagram we used only the quasars that have spectra with  $S/N > 5$  and we do not remove GRQs and SRQs from the DR14Q FIRST sample as they constitute only 1.6% and 2%, respectively, of the latter sample. In Figure 11, we also marked the division line between population A and population B at  $FWHM H\beta=4000$  km/s. It can be seen that most GRQs (91%), and SRQs (83%) belong to the B population. The objects in this region are massive, old galaxies with low accretion rates. The location of GRQs is typical for lobe-dominated quasars (Zamfir & Fan 2008), however few sources are located far off the main sequence area occupied by the lobe-dominated radio quasars. Two GRQs have extreme values of  $R_{FeII}$ : J2315+2518 and J1408+3054 as are two smaller-sized radio quasars: J1628+4552 and J1108+6451. The location of J1408+3054 can be explained by a large amount of out-flowing gas (Marziani et al. 2018), as this GRQ is a broad absorption line quasar. Spectral properties, as well as properties in other wavebands have to be studied in more detail to understand the specific positions of the remaining quasars in the EV1 plane.

The location of GRQs and SRQs in the EV1 plane is in agreement with the relation between BH masses ( $M_{BH}$ ) and Eddington ratio (the ratio of bolometric to Eddington luminosity,  $R_{Edd}=L_{bol}/L_{Edd}$ ) plotted in Figure 12. For all quasars studied in this paper, the estimation of BH masses, as well as the bolometric and Eddington luminosities, were taken from Rakshit et al. (2020). It can be clearly seen that GRQs and SRQs concentrate

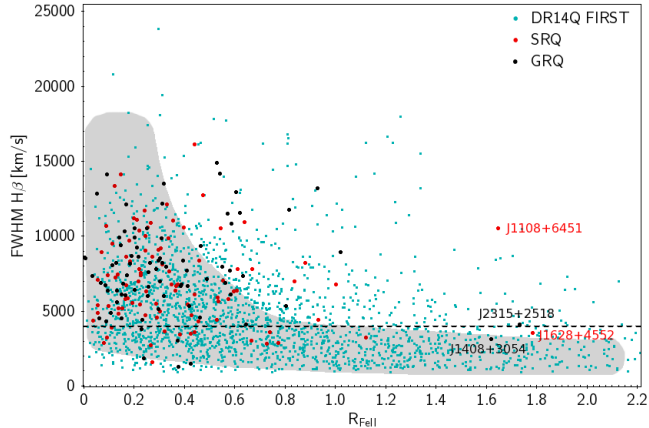


**Figure 11.** The Eigenvector 1 plane for GRQs (black dots), SRQs (red dots) and DR14Q quasars with FIRST counterparts (DR14Q FIRST; green dots). The horizontal line at  $\text{FWHM H}\beta=4000$  km/s separates two different populations of quasars: population A below  $\text{FWHM H}\beta=4000$  km/s and population B above the  $\text{FWHM H}\beta=4000$  km/s. The locations of the four extreme cases J1108+6451, J1628+4552, J1408+3054, J2315+2518 are marked. The shaded area indicatively traces the distribution of a quasar sample from Zamfir et al. (2010), defining the quasar main sequence.

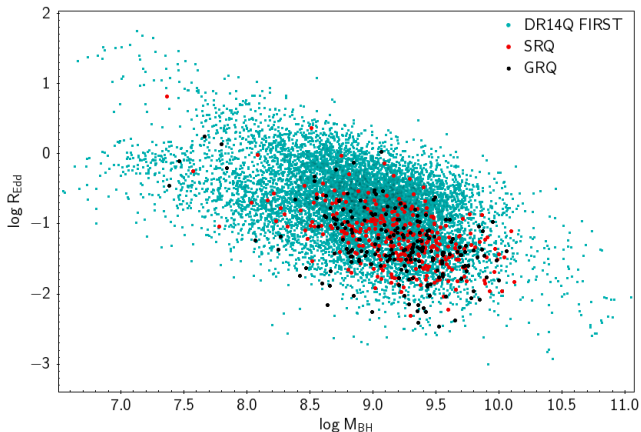


**Figure 12.** Eddington ratio vs. BH masses for GRQs, SRQs, and DR14Q FIRST quasars. The symbols are as in Figure 11.

in the region of larger  $M_{BH}$  and lower Eddington ratio as compared to the DR14Q FIRST quasars, which confirms that the extended radio quasars are evolved sources where accretion processes are not currently significant, representing later stages of evolution.

## 6. WISE COLOUR DIAGRAM

In this section, we study the infrared colours based on WISE magnitudes in W1, W2, and W3 bands at 3.4, 4.6 and 12  $\mu\text{m}$  respectively (Wright et al. 2010). W1-W2 and W2-W3 colours were used by Wright et al. (2010) for classification of astrophysical objects. Different classes

of objects occupy different parts on the colour-colour diagram. In our analysis we used infrared magnitudes given in the DR14Q catalogue, which are a result of cross-matching AllWISE Source Catalog (Cutri et al. 2013) with DR14Q FIRST quasars. We used only the magnitudes with A or B quality flags as listed for the 198 126 AllWISE matches we found for the 526 356 DR14Q quasars.

Almost all the quasars from the GRQ and SRQ samples were detected by WISE. We compared their colours with those of the quasars from DR14Q to check their position on the colour-colour diagram relative to the entire quasar population. In Figure 13, we can see that most quasars occupy the region centred at  $W1-W2\approx 1.1$  and  $W2-W3\approx 3.1$ . Such a position within the colour-colour diagram (according to Wright et al. 2010, Klindt et al. 2019, Wu et al. 2012) is characteristic for quasars. It can be seen that GRQs and SRQs occupy a smaller area than that of the quasars from DR14Q and that of the DR14Q FIRST quasars with FIRST detections, being concentrated within an ellipsoidal area in the upper left part of the diagram, with the central points of  $W1-W2=1$ ,  $W2-W3=2.7$  and the semi-major and semi-minor axes 0.8 and 0.3 respectively. The smaller area occupied by GRQs and SRQs coincides with the region of highest QSO density in DR14Q, and thus the region with the highest probability of finding quasars. However, when comparing the distributions of WISE colours for GRQs and DR14Q FIRST quasars (Figure 14), it is evident that GRQs have bluer W2-W3 colours, while W1-W2 colours for both the samples have similar distributions. The same behaviour is observed for the SRQ sample, which means that, as compared to the population of DR14Q FIRST quasars, GRQs and SRQs show a deficit of mid-infrared radiation towards longer wavelengths. This can indicate differences in the structure of the dusty torus (e.g. Wildy et al. 2018) which is responsible for mid-infrared re-emission of absorbed radiation from the central source. It can also be a result of lower star formation rate in GRQs and SRQs, as compared to DR14Q FIRST quasars (e.g. Klindt et al. 2019).

## 7. CONCLUDING REMARKS

In this study we present the basic properties of a sample of 272 GRQs, the largest yet constructed and comprised of 98 previously known ones, plus 174 GRQs newly discovered here using NVSS, FIRST and SDSS data. Among the new GRQs, there are 70 quasars at redshift  $z>1$ , of which 9 are located at  $z>2$ , with the most distant one, J1411+0156 at  $z=2.946$ . A large number of GRQs found by our thorough and time-consuming visual inspection of radio images proves that some of

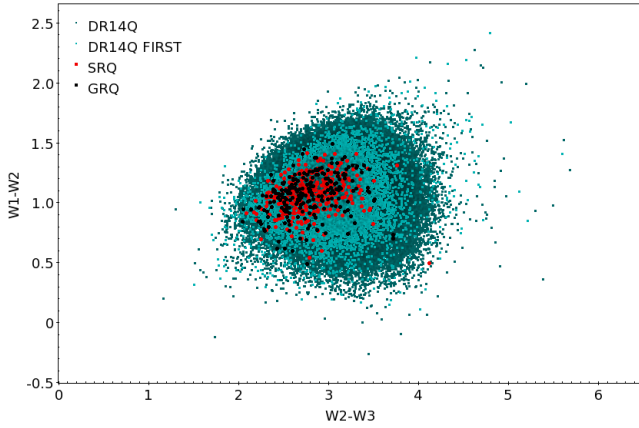


**Figure 13.** WISE colour-colour diagram for GRQs (black dots), SRQs (red dots), DR14Q (dark green dots), DR14Q FIRST (green dots).

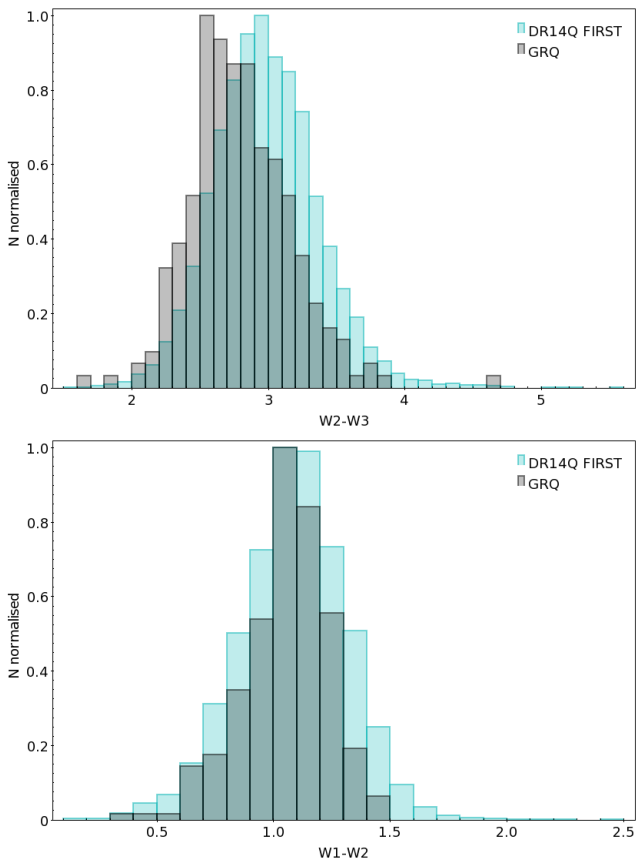


**Figure 14.** Normalized distributions of WISE colours for GRQ and SDSS DR14Q FIRST samples.

the modern/computer searches should be significantly modified. We enlarged the number of known GRQs nearly threefold, showing that previous catalogues of GRGs are incomplete and future extensive search is also necessitated for GRGs.

The search method used for the identification of GRQs also allowed us to compile a sample of 367 extended radio quasars with smaller radio structures ( $0.2 < D < 0.7$  Mpc), which can be used in other investigations. It contains only the quasars found in this work.

Our analysis of optical, radio and infrared host properties of GRQs, SRQs and quasars from the DR14Q FIRST sample gave the following results:

- The radio core prominence for GRQs and SRQs is just very weakly correlated with the EW of broad emission lines. We did not find either any statistically significant anticorrelation between EW of [OIII] and radio core prominence.
- We obtained a strong correlation between the [OIII] luminosity and the total and core radio luminosities for GRQs, as well as SRQs.
- Based on the position of quasars within the Eigenvector 1 plane, most of GRQs and SRQs belong to B population with  $\text{FWHM } H\beta > 4000$  km/s, representing evolved objects with high BH masses and the low accretion rates.
- There are few quasars in our samples with extreme values of EW FeII to EW  $H\beta$  ratio, compared to other GRQs and SRQs. They should be studied separately to understand their specific location in the Eigenvector 1 plane.
- The positions of GRQs and SRQs on the WISE colour-colour diagram show a deficit of mid-infrared radiation towards longer wavelengths, which may indicate differences in the structure of the dusty torus, as compared to quasars from DR14Q FIRST sample.

We found no significant differences between GRQs and SRQs, which show that in general the extended radio quasars are a group of objects with similar spectral and infrared properties. The size of radio structures seems to be independent of the host galaxies' spectral properties, while there is a strong connection between the radio luminosity and the [OIII] emission line emitted in the NLR. Also the infrared W2-W3 colours of both GRQs and SRQs have smaller values than those of DR14Q quasars in general, indicating differences in their dusty torus structure.

## 8. ACKNOWLEDGMENTS

We thank the referee for valuable comments and corrections that helped to improve the paper. We also thank Conor Wildy for his helpful comments.

This paper was supported by the National Science Centre, Poland through the grant 2018/29/B/ST9/01793.

## REFERENCES

- Baum, S. A., & Heckman, T. M., 1989, *ApJ*, 336, 702
- Becker, R. H., White, R. L., Helfand, D. J., 1995, *ApJ*, 450, 559
- Baker, J. C., 1997, *MNRAS*, 286, 23
- Boroson, T. A., & Green, R. F., 1992, *ApJS*, 80, 109
- Brown, M. J. I., Webster, R. L., Boyle, B. J., 2001, *AJ*, 121, 2381
- Browne, I. W. A., & Murphy, D. W., 1987, *MNRAS*, 226, 601
- Condon, J. J., Cotton, W. D., Greisen, E. W., Yin, Q. F., 1998, *AJ*, 115, 1693
- Coziol, R., Andernach, H., Torres-Papaqui, J. P., Ortega-Minakata, R. A., Moreno del Rio, F., 2017, *MNRAS*, 466, 921
- Cutri, R. M., Wright, E. L., & Conrow, T. 2013, Explanatory Supplement to the ALLWISE Data Release Products, Tech. Rep. (Pasadena, CA: Caltech)
- Dabhade, P., Gaikwad, M., Bagchi, J., et al., 2017, *MNRAS*, 469, 2886
- Dabhade, P., Röttgering, H. J. A., Bagchi, J., et al., 2020a, *A&A*, 635, 5
- Dabhade, P., Mahato, M., Bagchi, J., et al., 2020b, *A&A*, 642, 153
- Dunlop, J. S., & Peacock, J. A., 1993, *MNRAS*, 263, 93
- Flewelling, H. A., Magnier, E. A., Chambers, K. C., et al., 2020, *ApJS*, 251, 7
- Gaur, H., Gu, M., Ramya, S., Guo, H., 2019, *A&A*, 631, 46
- Ghisellini, G., Celotti, A., Tavecchio, F., Haardt, F., Sbarrato, T., 2014, *MNRAS*, 438, 2694
- Intema, H. T., Jagannathan, P., Mooley, K. P., Frail, D. A., 2017, *A&A*, 598, 78
- Ishwara-Chandra, C. H., & Saikia, D. J., 1999, *MNRAS*, 309, 100
- Jackson, N., Browne, I. W. A., Murphy, D. W., Saikia, D. J., 1989, *Nature*, 338, 485
- Jackson, N., & Browne, I. W. A., 1991, *MNRAS*, 250, 422
- Jackson, N., & Browne, I. W. A., 2013, *MNRAS*, 429, 1781
- Jamrozy, M., Konar, C., Machalski, J., Saikia, D. J., 2008, *MNRAS*, 385, 1286
- Kaiser, C. R., Dennett-Thorpe, J., Alexander, P., 1997, *MNRAS*, 292, 723
- Kharb, P., & Shastri, P., 2004, *A&A*, 425, 825
- Kimball, A. E., Ivezić, Ž., Wiita, P. J., Schneider, D. P., 2011, *ApJ*, 141, 182
- Klindt, L., Alexander, D. M., Rosario, D. J., Lusso, E., Fotopoulou, S., 2019, *MNRAS*, 488, 3109
- Konar, C., Jamrozy, M., Saikia, D. J., Machalski, J., 2008, *MNRAS*, 383, 525
- Kozieł-Wierzbowska, D., Goyal, A., Żywucka, N., 2020, *ApJS*, 247, 53
- Kuligowska, E., Jamrozy, M., Kozieł-Wierzbowska, D., Machalski, J., 2009, *AcA*, 59, 431
- Kuźmicz, A., & Jamrozy, M., 2012, 426, 851
- Kuźmicz, A., Jamrozy, M., Kozieł-Wierzbowska, D., Weźgowiec, M., 2017, *MNRAS*, 471, 3806
- Kuźmicz, A., Jamrozy, M., Bronarska, K., Janda-Boczar, K., Saikia, D. J., 2018, *ApJS*, 238, 9
- Kuligowska, E., & Kuźmicz, A., 2018, *PAS*, 7, Proceedings of the Polish Astronomical Society, ed. A. Różańska, 82
- Lacy, M., Baum, S. A., Chandler, C. J., et al., 2020, *PASP*, 132, 5001
- Laing, R. A., Riley, J. M., Longair, M. S., 1983, *MNRAS*, 204, 151
- Machalski, J., Jamrozy, M., Saikia, D. J., 2009, *MNRAS*, 395, 812
- Marziani, P., Sulentic, J. W., Zwitter, T., et al., 2001, *ApJ*, 558, 553
- Marziani, P., Dultzin, D., Sulentic, J. W., et al., 2018, *FrASS*, 5, 6
- Miller, P., Rawlings, S., Saunders, R., 1999, *MNRAS*, 263, 425
- Nenkova, M., Sirocky, M. M., Nikutta, R., Ivezić, Ž., Elitzur, M., 2008, *ApJ*, 685, 160
- Netzer, H., 1987, *MNRAS*, 225, 55
- Olmo, A., Marziani, P., Ganci, V., et al., 2020, arXiv: 2004.12748
- Orr, M. J. L., & Browne, I. W. A., 1982, *MNRAS*, 200, 1067
- Pâris, I., Petitjean, P., Aubourg É., et al., 2018, *A&A*, 613, 51
- Proctor, D. D., 2016, *ApJS*, 224, 18
- Rakshit, S., Stalin, C. S., Kotilainen, J., 2020, *ApJS*, 249, 17
- Rawlings, S., Saunders, R., Eales, S. A., Mackay, C. D., 1989, *MNRAS*, 240, 701
- Rawlings, S., & Saunders, R., 1991, *Nat*, 349, 138
- Rosen, S. R., Webb, N. A., Watson, M. G., et al. 2016, *A&A*, 590, 1
- Schlafly, E. F., Meisner, A. M., Green, G. M., 2019, *ApJS*, 240, 30



- Shimwell, T. W., Röttgering, H. J. A., Best, P. N., et al., 2017, *A&A*, 598, 104
- Shimwell, T. W., Tasse, C., Hardcastle, M. J., et al., 2019, *A&A*, 622, 1
- Simionescu, A., Stawarz, L., Ichinohe, Y., et al., 2016, *ApJL*, 816, 15
- Spergel, D. N., Verde, L., Peiris, H. V., et al., 2003, *ApJS*, 148, 175
- Subrahmanyan, R., Saripalli, L., Safouris, V., Hunstead, R. W., 2008, *ApJ*, 677, 63
- Sulentic, J. W., Marziani, P., Zamanov, R., et al., 2002, *ApJ*, 566, 71
- Sulentic, J. W., del Olmo, A., Marziani, P., et al., 2017, *A&A*, 608, A122
- Tadhunter, C. N., Morganti, R., Robinson, A., et al., 1998, *MNRAS*, 298, 1035
- Voges, W., Aschenbach, B., Boller, T., et al., 1999, *A&A*, 349, 389
- Voges, W., Aschenbach, B., Boller, T., et al., 2000, *IAU Circ.*, 743
- Wardle, J. F. C., & Aaron, S. E., 1997, *MNRAS*, 286, 425
- Wildy, C., Czerny, B., Kuźmich, A., 2018, *ApJ*, 861, 5
- Willott, C. J., Rawlings, S., Blundell, K. M., Lacy, M., 1999, *MNRAS*, 309, 1017
- Wright, E. L., Eisenhardt, P. R. M., Mainzer, A. K., et al., 2010, *AJ*, 140, 1868
- Wu, X.-B., Hao, G., Jia, Z., Zhang, Y., Peng, N., 2012, *AJ*, 144, 49
- Zamfir, S., Sulentic, J. W., Marziani, P., 2008, *MNRAS*, 387, 856
- Zamfir, S., Sulentic, J. W., Marziani, P., Dultzin, D., 2010, *MNRAS*, 403, 1759
- Zhang, J. S., & Fan, J. H., 2003, *Chin. J. Astron. Astrophys.*, 3, 415

NOTE— **Column description:** (1) – source name, (2) and (3) – J2000.0 source coordinates, (4) – redshift, (5) – angular size; measured on FIRST maps as a distance between hot-spots, (6) – projected linear size, (7) – radio core prominence, (8) core radio luminosity at 1.4 GHz in units of W/Hz, (9) – total radio luminosity at 1.4 GHz in units of W/Hz, (10) – flag: (fn) – angular size for radio sources with FIRST radio structure visible only on the one side; measured between the FIRST hot-spot on the one side and the maximum of NVSS emission on the other side, (nn) – angular size for radio sources with no visible FIRST hot-spots; measured between maxima of NVSS emission, (v) – angular size for radio source with no visible FIRST hot-spots; measured between hot-spots detected in VLASS, (s) – the total radio luminosity is affected by a background radio source. We subtracted 8 mJy VLASS 3 GHz contaminating source assuming the spectral index  $\alpha=-0.7$ , (c) – candidate GRQ with uncertain radio morphology, (h) – uncertain host position, the galaxy SDSS J142302.67+265014.9 located at redshift  $z_{\text{phot}}=0.7$  is also a possible host, (j) – the quasars with visible one-sided radio jet (Section 2.4).

**Table 1.** List of 174 newly discovered GRQs.

IAU name	$\alpha(2000)$ (h m s)	$\delta(2000)$ ( $^{\circ}$ ' ")	z	LAS <sub>FIRST</sub> (arcmin)	D <sub>FIRST</sub> (Mpc)	f <sub>c</sub>	logP <sub>core</sub> W Hz <sup>-1</sup>	logP <sub>tot</sub> W Hz <sup>-1</sup>	Flag
(1)	(2)	(3)	(4)	(5)	(6)	(7)	(8)	(9)	(10)
J0012+0902	00 12 09.85	+09 02 49.3	0.7930	1.90	0.85	0.06	24.85	26.18	
J0023-0926	00 23 34.07	-09 26 24.3	0.7886	2.71	1.22	0.03	24.14	25.76	
J0024+0057	00 24 22.62	+00 57 51.2	0.9646	1.50	0.72	0.02	23.84	25.74	
J0032+2327	00 32 10.51	+23 27 55.0	0.6393	2.83	1.17	-	-	25.49	v
J0032+1852	00 32 17.09	+18 52 56.1	0.5307	2.99	1.13	-	-	25.73	v
J0032-0605	00 32 46.62	-06 05 33.9	0.7540	3.96	1.75	0.34	25.28	25.95	fn
J0034+3330	00 34 45.88	+33 30 18.6	2.2270	1.71	0.86	-	-	27.29	v
J0043+3137	00 43 59.87	+31 37 20.3	0.6266	3.01	1.23	-	-	26.24	v
J0050-0234	00 50 48.73	-02 34 17.1	1.4312	2.46	1.25	2.11	25.80	26.09	fn
J0051-0902	00 51 15.12	-09 02 08.5	1.2650	1.46	0.73	0.02	24.39	26.18	
J0053-0210	00 53 12.61	-02 10 14.5	1.3062	1.39	0.70	0.02	24.50	26.39	
J0105+0100	01 05 47.28	+01 00 58.8	0.9590	1.55	0.74	0.06	24.39	25.74	
J0116+1054	01 16 38.08	+10 54 49.1	0.7270	2.93	1.27	0.07	24.44	25.72	
J0116+1829	01 16 39.17	+18 29 14.9	1.3853	1.56	0.80	-	-	27.04	v
J0136+3119	01 36 35.68	+31 19 12.9	0.7080	2.21	0.95	-	-	25.87	v,s
J0137+0034	01 37 48.19	+00 34 02.3	0.7975	1.78	0.80	0.00	24.13	26.74	
J0156-0253	01 56 36.34	-02 53 47.3	1.7329	1.46	0.75	0.20	25.69	26.60	
J0229-0008	02 29 30.92	-00 08 45.4	0.6088	2.50	1.01	0.34	25.34	25.99	
J0235+0329	02 35 19.69	+03 29 00.0	0.7411	1.79	0.78	0.10	25.11	26.22	
J0249-0340	02 49 24.71	-03 40 24.4	0.8480	1.68	0.77	1.05	25.70	26.07	
J0314-0750	03 14 13.73	-07 50 23.8	1.2495	1.85	0.93	0.07	25.58	26.88	
J0758+3556	07 58 58.30	+35 56 43.7	0.7468	2.36	1.04	0.12	24.76	25.81	
J0804+2722	08 04 59.95	+27 22 48.7	0.5788	2.32	0.91	0.01	24.21	26.12	
J0811+1652	08 11 45.87	+16 52 56.4	2.1620	1.38	0.70	0.08	25.37	26.65	
J0813+2057	08 13 53.10	+20 57 51.2	0.9033	3.08	1.45	0.04	24.34	25.83	

Table 1 continued

Table 1 (continued)

IAU name (1)	$\alpha(2000)$ (h m s) (2)	$\delta(2000)$ ( $^{\circ}$ ' ") (3)	$z$ (4)	LAS <sub>FIRST</sub> (arcmin) (5)	D <sub>FIRST</sub> (Mpc) (6)	$f_c$ (7)	$\log P_{\text{core}}$ W Hz <sup>-1</sup> (8)	$\log P_{\text{tot}}$ W Hz <sup>-1</sup> (9)	Flag (10)
J0820+1958	08 20 09.29	+19 58 23.1	0.9910	1.72	0.83	0.01	23.95	26.02	
J0821+2030	08 21 31.19	+20 30 30.8	0.6526	4.45	1.85	0.14	24.61	25.59	
J0826+1909	08 26 58.57	+19 09 21.5	0.4281	3.51	1.17	0.36	24.69	25.32	fn
J0827+3747	08 27 20.71	+37 47 06.7	0.8274	1.58	0.72	0.04	24.50	26.00	
J0838+1358	08 38 13.13	+13 58 10.6	2.0277	2.35	1.20	0.17	26.08	27.06	
J0838+1022	08 38 56.38	+10 22 01.0	0.5925	4.56	1.81	0.15	24.69	25.63	
J0844+0830	08 44 41.51	+08 30 59.9	0.7044	2.39	1.03	0.13	25.28	26.29	
J0846+1413	08 46 36.11	+14 13 07.8	0.4929	2.71	1.00	0.03	24.64	26.26	
J0847+0217	08 47 49.24	+02 17 14.9	0.5089	2.21	0.81	0.13	24.10	25.09	fn
J0849+4216	08 49 40.11	+42 16 04.3	0.9559	1.54	0.73	0.18	24.56	25.47	fn
J0854-0011	08 54 59.98	-00 11 00.2	0.7680	2.16	0.96	0.02	24.60	26.32	
J0859+3031	08 59 21.11	+30 31 20.1	0.8720	1.62	0.75	0.03	24.24	25.86	
J0859+3506	08 59 40.29	+35 06 47.4	1.3895	1.38	0.70	0.02	24.93	26.67	
J0906+0111	09 06 04.03	+01 11 14.2	0.7981	3.45	1.56	0.08	24.68	25.86	
J0906+6009	09 06 19.83	+60 09 45.3	1.1675	1.50	0.75	0.28	25.79	26.55	
J0920+6147	09 20 27.84	+61 47 00.8	0.7480	3.36	1.48	0.10	24.77	25.88	
J0926+4722	09 26 28.90	+47 22 36.1	2.0000	1.98	1.01	0.07	25.56	26.91	
J0927+3431	09 27 51.12	+34 31 03.6	0.4260	3.11	1.04	0.16	24.61	25.52	
J0931+1751	09 31 41.26	+17 51 56.5	0.9709	2.08	0.99	0.09	24.60	25.79	
J0932+0742	09 32 56.81	+07 42 12.2	1.0037	2.23	1.08	1.48	25.94	26.25	
J0935+2214	09 35 04.64	+22 14 54.4	0.7804	1.78	0.80	0.01	24.44	26.44	
J0942+1245	09 42 16.52	+12 45 03.7	1.4338	1.59	0.82	0.31	25.92	26.66	
J0945+2506	09 45 04.70	+25 06 05.1	1.0949	1.81	0.89	0.05	24.80	26.26	
J0948+4719	09 48 03.64	+47 19 28.9	1.6600	1.97	1.01	0.02	24.70	26.65	
J0958+4608	09 58 19.33	+46 08 25.6	0.6415	1.88	0.78	0.03	24.44	26.06	
J1007+1652	10 07 51.16	+16 52 43.4	0.4855	2.33	0.85	0.08	24.65	25.84	
J1011+0503	10 11 26.20	+05 03 03.8	0.7550	1.84	0.81	0.72	25.37	25.82	fn
J1014+6047	10 14 02.40	+60 47 24.6	0.6725	3.08	1.30	0.23	24.71	25.50	fn
J1017+4705	10 17 54.86	+47 05 29.1	0.6680	2.33	0.99	0.47	25.05	25.62	
J1020-0247	10 20 03.00	-02 47 16.6	1.4470	1.65	0.80	0.06	25.64	27.01	
J1029+2103	10 29 34.00	+21 03 45.8	0.8240	2.43	1.11	0.04	24.93	26.41	
J1033+1508	10 33 48.23	+15 08 15.4	0.5794	4.76	1.87	0.22	24.93	25.73	
J1038+1346	10 38 22.48	+13 46 57.3	0.9470	1.71	0.82	1.87	26.12	26.40	
J1045+4040	10 45 25.67	+40 40 36.9	1.0911	2.11	1.04	0.18	25.16	26.07	
J1046+5738	10 46 04.21	+57 38 18.4	1.3536	2.07	1.05	0.21	25.89	26.76	j

Table 1 continued

Table 1 (*continued*)

IAU name	$\alpha(2000)$ (h m s)	$\delta(2000)$ ( $^{\circ}$ ' ")	$z$	LAS <sub>FIRST</sub> (arcmin)	D <sub>FIRST</sub> (Mpc)	$f_c$	$\log P_{\text{core}}$ W Hz $^{-1}$	$\log P_{\text{tot}}$ W Hz $^{-1}$	Flag
(1)	(2)	(3)	(4)	(5)	(6)	(7)	(8)	(9)	(10)
J1048+3209	10 48 51.81	+32 09 03.1	0.8313	2.11	0.96	0.05	25.10	26.50	j
J1054-0107	10 54 43.14	-01 07 01.8	0.5222	2.15	0.80	0.00	23.38	26.53	
J1056+2743	10 56 37.97	+27 43 43.6	0.9991	1.66	0.81	0.05	25.71	27.16	
J1058+4458	10 58 40.72	+44 58 15.1	2.4450	1.49	0.74	-	-	26.91	
J1100+2314	11 00 01.14	+23 14 13.2	0.5565	2.20	0.85	0.07	25.13	26.38	
J1106+6247	11 06 55.98	+62 47 59.9	0.8440	2.48	1.14	0.22	25.16	25.98	
J1120+1104	11 20 21.37	+11 04 34.8	0.4955	2.56	0.93	0.49	25.56	26.09	
J1120+2140	11 20 54.11	+21 40 38.1	1.5310	3.24	1.66	0.45	25.29	25.92	
J1127+4534	11 27 59.93	+45 34 17.6	2.2930	1.90	0.95	0.18	25.51	26.49	
J1129+4025	11 29 56.02	+40 25 14.4	0.7580	2.80	1.24	0.02	24.27	26.01	
J1133+6035	11 33 23.03	+60 35 00.2	0.9691	2.64	1.26	0.92	25.24	25.65	fn
J1136+3516	11 36 45.59	+35 16 36.5	1.7750	3.03	1.55	0.03	25.15	26.80	
J1145+4423	11 45 59.45	+44 23 50.7	1.2694	1.41	0.71	0.24	25.97	26.79	j
J1146+3345	11 46 03.76	+33 45 52.0	0.7610	1.90	0.84	0.03	24.58	26.18	
J1147+2619	11 47 31.38	+26 19 50.0	1.7500	1.49	0.76	0.02	24.68	26.60	
J1149+1420	11 49 27.98	+14 20 02.3	0.3772	4.11	1.27	0.09	24.22	25.36	fn
J1151+1926	11 51 41.51	+19 26 09.9	0.5967	4.41	1.76	0.20	24.68	25.52	
J1158+1402	11 58 34.87	+14 02 11.4	0.4705	2.41	0.85	0.11	24.08	25.14	fn
J1159+2106	11 59 26.21	+21 06 55.9	0.3470	2.95	0.86	0.02	24.20	25.97	
J1208+2219	12 08 22.00	+22 19 58.3	0.7448	1.90	0.84	0.05	25.13	26.53	
J1209+1635	12 09 28.58	+16 35 23.2	0.9750	2.38	1.14	1.10	25.74	26.11	
J1213+2237	12 13 39.69	+22 37 20.1	1.0449	2.12	1.04	0.11	25.07	26.16	
J1213+0832	12 13 57.15	+08 32 02.3	0.8110	2.85	1.29	0.26	25.32	26.08	
J1214+1828	12 14 31.16	+18 28 14.9	1.5858	1.53	0.79	0.16	26.18	27.17	
J1219+1741	12 19 44.72	+17 41 21.0	1.5147	1.98	1.02	0.11	25.37	26.47	
J1225+2547	12 25 40.12	+25 47 24.6	0.8090	1.64	0.74	0.17	25.04	25.96	
J1229+6242	12 29 40.90	+62 42 54.7	0.9670	1.74	0.83	0.32	25.49	26.19	
J1232+2037	12 32 47.42	+20 37 45.2	0.5673	2.66	1.04	0.21	24.94	25.76	
J1237+5448	12 37 35.89	+54 48 14.5	1.0284	2.47	1.20	0.56	25.11	25.65	
J1241+6038	12 41 38.93	+60 38 31.7	0.9986	1.77	0.85	0.28	24.98	25.73	fn
J1252+4848	12 52 34.67	+48 48 58.7	1.8400	1.78	0.91	0.87	26.21	26.68	c
J1255+0841	12 55 43.17	+08 41 45.3	0.8141	1.68	0.76	0.01	23.83	25.88	
J1257+4054	12 57 10.83	+40 54 29.5	1.0681	2.02	1.00	0.09	25.01	26.20	
J1304+1811	13 04 52.78	+18 11 09.0	1.2990	1.77	0.90	0.29	25.76	26.51	
J1305+2408	13 05 44.58	+24 08 40.9	0.4545	2.45	0.85	0.22	24.48	25.28	fn

Table 1 *continued*



Table 1 (*continued*)

IAU name (1)	$\alpha(2000)$ (h m s) (2)	$\delta(2000)$ ( $^{\circ}$ ' ") (3)	$z$ (4)	LAS <sub>FIRST</sub> (arcmin) (5)	D <sub>FIRST</sub> (Mpc) (6)	$f_c$ (7)	$\log P_{\text{core}}$ W Hz <sup>-1</sup> (8)	$\log P_{\text{tot}}$ W Hz <sup>-1</sup> (9)	Flag (10)
J1307+1438	13 07 42.14	+14 38 40.3	1.0702	2.82	1.38	0.29	24.86	25.60	
J1309+4232	13 09 10.32	+42 32 24.9	0.7600	1.65	0.73	0.04	24.08	25.62	
J1316+2720	13 16 25.01	+27 20 42.7	0.6910	2.37	1.01	0.08	24.58	25.79	
J1329+4803	13 29 19.42	+48 03 00.6	1.5970	2.24	1.15	0.03	25.34	26.96	
J1330+5731	13 30 41.61	+57 31 29.7	0.6259	1.88	0.77	0.81	24.93	25.34	
J1331+2500	13 31 27.82	+25 00 50.1	0.8039	1.67	0.76	0.01	24.95	27.01	
J1333+0450	13 33 07.00	+04 50 48.5	1.4050	2.21	1.14	0.12	25.63	26.72	
J1343+2057	13 43 58.09	+20 57 13.4	1.6610	2.18	1.12	0.96	25.90	26.34	
J1356+1904	13 56 00.05	+19 04 21.0	2.2350	1.58	0.80	0.51	26.32	26.95	
J1401+5651	14 01 58.54	+56 51 57.7	0.6290	1.78	0.73	0.08	24.53	25.71	
J1408+1010	14 08 13.86	+10 10 13.7	0.4528	2.29	0.80	0.002	23.83	26.68	
J1408+3834	14 08 27.52	+38 34 35.3	1.2760	1.67	0.84	1.66	25.66	25.97	
J1410+6327	14 10 01.39	+63 27 39.9	1.9464	1.89	0.96	0.36	25.80	26.51	
J1411+0156	14 11 39.88	+01 56 16.5	2.9460	2.64	1.25	0.33	26.14	26.92	c
J1412+2021	14 12 13.32	+20 21 07.1	1.9050	3.20	1.63	0.23	25.65	26.52	
J1412+2326	14 12 57.78	+23 26 19.1	0.4599	2.18	0.76	0.21	24.73	25.54	c
J1414+5549	14 14 12.80	+55 49 37.9	0.3011	2.70	0.72	0.07	23.19	24.43	
J1423+2650	14 23 03.30	+26 50 10.8	0.7810	2.10	0.94	0.01	24.00	25.96	h
J1424+6113	14 24 51.86	+61 13 07.4	1.0449	3.08	1.50	0.53	25.43	25.99	
J1426+0256	14 26 32.38	+02 56 45.4	0.8611	3.54	1.64	3.25	25.92	26.11	
J1427+3625	14 27 18.21	+36 25 01.1	0.8509	2.45	1.13	0.20	25.13	26.00	
J1429+3356	14 29 42.65	+33 56 54.8	1.1215	2.12	1.05	0.22	25.14	25.98	
J1432+5200	14 32 58.48	+52 00 05.8	1.5130	1.81	0.93	0.43	25.35	25.99	c
J1437+0748	14 37 47.72	+07 48 56.5	1.4747	1.61	0.83	0.05	25.36	26.82	
J1439+4550	14 39 32.67	+45 50 28.6	1.8190	1.48	0.76	0.16	25.53	26.52	
J1440+2607	14 40 30.07	+26 07 46.2	0.8080	3.00	1.36	0.17	24.65	25.57	fn
J1441+2216	14 41 32.21	+22 16 35.7	0.3340	3.21	0.92	0.07	24.49	25.74	j
J1444+0737	14 44 57.10	+07 37 57.9	1.0550	1.78	0.88	0.10	25.23	26.36	
J1445+1944	14 45 08.45	+19 44 50.4	1.4523	1.74	0.89	0.03	24.94	26.59	
J1449-0131	14 49 27.42	-01 31 06.4	0.5592	2.15	0.83	0.12	24.78	25.82	
J1450+4549	14 50 38.83	+45 49 54.6	1.6207	1.59	0.82	0.09	25.92	27.13	
J1451+1141	14 51 03.24	+11 41 08.5	1.0671	1.54	0.76	0.38	25.69	26.35	
J1453+2217	14 53 08.00	+22 17 07.5	0.7846	2.02	0.92	0.15	25.48	26.45	
J1453+4518	14 53 28.17	+45 18 01.2	0.6033	3.66	1.47	0.19	24.74	25.61	
J1454+6154	14 54 09.56	+61 54 02.1	2.0820	1.75	0.89	0.04	25.05	26.62	

Table 1 *continued*

Table 1 (*continued*)

IAU name (1)	$\alpha(2000)$ (h m s) (2)	$\delta(2000)$ ( $^{\circ}$ ' ") (3)	$z$ (4)	LAS <sub>FIRST</sub> (arcmin) (5)	D <sub>FIRST</sub> (Mpc) (6)	$f_c$ (7)	$\log P_{\text{core}}$ W Hz <sup>-1</sup> (8)	$\log P_{\text{tot}}$ W Hz <sup>-1</sup> (9)	Flag (10)
J1507+1104	15 07 39.49	+11 04 03.9	0.4755	2.40	0.86	0.04	24.73	26.21	
J1514+5559	15 14 41.13	+55 59 32.8	1.1900	1.71	0.86	0.01	24.07	26.04	
J1516+2741	15 16 16.85	+27 41 22.9	0.7460	3.36	1.48	0.36	24.85	25.50	fn
J1518+4832	15 18 30.93	+48 32 14.5	0.5758	2.18	0.86	0.08	24.66	25.86	
J1520+1253	15 20 56.73	+12 53 46.9	0.6570	2.54	1.06	0.07	24.11	25.35	fn
J1524+3335	15 24 57.34	+33 35 00.9	0.9035	2.45	1.15	0.03	24.51	26.11	
J1525+3010	15 25 53.55	+30 10 23.3	1.1920	1.98	0.99	0.24	25.10	25.91	
J1525+5916	15 25 56.25	+59 16 59.1	0.9551	1.91	0.92	0.10	25.56	26.68	
J1532+1234	15 32 17.57	+12 34 00.1	0.7490	1.99	0.88	0.29	24.69	25.41	fn
J1532+1110	15 32 24.64	+11 10 18.8	1.1473	1.92	0.96	0.14	25.50	26.53	
J1533+0658	15 33 13.21	+06 58 01.6	1.1600	1.61	0.81	0.94	26.18	26.59	j
J1540+0132	15 40 47.88	+01 32 06.8	0.7739	1.64	0.74	0.35	25.41	26.08	
J1542+1946	15 42 46.51	+19 46 26.1	0.3990	2.45	0.79	0.05	24.28	25.63	
J1552+0012	15 52 21.45	+00 12 56.9	1.4557	1.41	0.72	0.02	24.59	26.55	
J1553+2926	15 53 55.79	+29 26 36.8	1.1670	1.61	0.80	0.04	24.61	26.11	
J1554+4643	15 54 19.05	+46 43 32.4	1.4330	1.48	0.76	0.97	25.95	26.37	
J1601+1754	16 01 51.59	+17 54 09.9	0.6602	1.81	0.77	0.04	24.87	26.41	
J1603+3659	16 03 34.13	+36 59 53.0	0.9654	2.66	1.27	0.13	25.23	26.25	fn
J1606+1224	16 06 32.05	+12 24 16.3	1.3088	1.44	0.73	0.03	24.55	26.24	
J1609+5354	16 09 13.19	+53 54 29.7	0.9926	1.79	0.86	0.68	26.16	26.64	
J1609+4334	16 09 53.42	+43 34 11.5	0.7597	2.39	1.06	0.07	25.58	26.85	
J1613+3214	16 13 49.89	+32 14 01.4	0.7110	2.33	1.01	0.05	24.01	25.39	fn
J1616+4956	16 16 01.73	+49 56 34.4	1.7210	2.69	1.38	0.39	26.11	26.80	
J1618+2826	16 18 16.14	+28 26 10.5	0.8450	1.99	0.92	0.03	24.08	25.73	
J1619+3730	16 19 35.17	+37 30 49.4	0.9880	2.15	1.03	0.15	24.70	25.68	fn
J1619+4359	16 19 46.29	+43 59 15.3	0.8525	1.51	0.70	0.17	24.86	25.79	
J1622+3640	16 22 00.48	+36 40 44.0	1.9990	2.16	1.10	0.08	25.42	26.68	
J1623+2735	16 23 46.41	+27 35 13.6	1.3961	1.63	0.84	2.98	26.58	26.82	
J1628+5438	16 28 03.70	+54 38 44.7	1.3630	2.41	1.23	0.09	24.82	26.03	
J1647+3432	16 47 49.16	+34 32 53.0	0.7230	1.71	0.74	-	-	25.86	
J1649+3046	16 49 28.88	+30 46 52.4	1.1209	1.84	0.92	0.68	26.28	26.78	
J1706+3615	17 06 34.13	+36 15 08.0	0.9170	2.33	1.10	1.17	25.71	26.06	
J1707+2711	17 07 22.27	+27 11 32.0	1.5140	1.52	0.78	0.03	25.02	26.71	
J1714+2759	17 14 48.19	+27 59 19.1	0.9649	1.66	0.79	0.08	24.81	26.05	
J2127-0814	21 27 32.60	-08 14 45.5	1.0106	1.80	0.87	0.02	24.29	26.05	

Table 1 *continued*

**Table 1** (*continued*)

IAU name	$\alpha(2000)$ (h m s)	$\delta(2000)$ ( $^{\circ}$ ' ")	$z$	LAS <sub>FIRST</sub> (arcmin)	D <sub>FIRST</sub> (Mpc)	$f_c$	$\log P_{\text{core}}$ W Hz <sup>-1</sup>	$\log P_{\text{tot}}$ W Hz <sup>-1</sup>	Flag
(1)	(2)	(3)	(4)	(5)	(6)	(7)	(8)	(9)	(10)
J2145+1115	21 45 18.78	+11 15 27.3	0.5480	1.82	0.70	1.40	26.32	26.61	j
J2157+1936	21 57 37.33	+19 36 29.8	1.0324	1.68	0.82	-	-	25.54	nn
J2241+2732	22 41 02.03	+27 32 59.4	0.4935	4.86	1.76	-	-	26.32	v
J2248-1015	22 48 17.51	-10 15 47.1	0.2919	3.79	0.99	1.77	24.65	24.88	fn
J2254+1813	22 54 17.43	+18 13 01.0	1.4730	2.66	1.36	-	-	27.19	v
J2310+2452	23 10 15.58	+24 52 46.3	1.1573	2.42	1.20	-	-	26.12	nn
J2315+2518	23 15 50.98	+25 18 33.0	0.7734	1.81	0.81	-	-	25.74	nn
J2327+1533	23 27 35.98	+15 33 09.6	0.9880	2.44	1.17	-	-	26.43	nn
J2348+1529	23 48 07.68	+15 29 36.7	0.6810	2.22	0.94	-	-	25.95	v

NOTE—The column description and symbols meaning as in Table 1.  
 Angular size of sources which can not be measured in FIRST and VLASS radio maps are measured to the  $3\sigma$  contour level in NVSS maps, therefore their sizes may be overestimated. Such quasars are marked by (\*).

**Table 2.** List of 367 newly found SRQs.

IAU name	$\alpha(2000)$ (h m s)	$\delta(2000)$ ( $^{\circ}$ ' ")	z	LAS <sub>FIRST</sub> (arcmin)	D <sub>FIRST</sub> (Mpc)	$f_c$	$\log P_{\text{core}}$ W Hz <sup>-1</sup>	$\log P_{\text{tot}}$ W Hz <sup>-1</sup>	Flag
(1)	(2)	(3)	(4)	(5)	(6)	(7)	(8)	(9)	(10)
J0001+2452	00 01 26.18	+24 52 09.5	1.4230	1.34	0.68	-	-	26.36	v
J0007-0051	00 07 17.82	-00 51 37.8	0.5259	1.66	0.62	0.03	23.70	25.26	fn
J0010+3329	00 10 25.63	+33 29 36.8	0.7420	1.23	0.54	-	-	27.00	nn
J0014+0039	00 14 28.74	+00 39 04.7	1.1630	1.00	0.50	0.12	25.27	26.34	
J0015+0400	00 15 53.74	+04 00 39.6	0.7590	1.23	0.55	0.10	25.12	26.23	
J0022+2833	00 22 16.36	+28 33 54.9	0.5846	1.55	0.66	0.04	25.16	25.59	
J0022-0145	00 22 44.30	-01 45 50.9	0.6899	1.55	0.66	0.04	25.16	26.62	
J0029+1527	00 29 28.20	+15 27 22.4	0.7094	1.55	0.67	-	-	25.53	nn
J0039+3406	00 39 57.32	+34 06 45.0	0.7350	0.86	0.37	-	-	26.45	v
J0040+2520	00 40 30.68	+25 20 06.4	0.8220	0.93	0.42	-	-	26.37	nn
J0040+1503	00 40 39.79	+15 03 21.2	0.8844	0.92	0.43	0.32	25.57	26.26	
J0053+0223	00 53 46.23	+02 23 28.6	1.1421	1.18	0.59	-	-	26.67	
J0054+2603	00 54 24.30	+26 03 49.6	1.1586	1.29	0.65	-	-	26.64	v
J0058+2848	00 58 45.29	+28 48 58.4	0.8930	1.29	0.60	-	-	26.14	nn
J0108+2710	01 08 21.19	+27 10 47.8	1.5732	1.63	0.84	-	-	26.60	*
J0109+1447	01 09 31.40	+14 47 29.2	2.0658	0.81	0.41	-	-	26.71	v
J0117+2212	01 17 16.21	+22 12 15.9	1.5015	0.83	0.43	-	-	26.95	v
J0118+2248	01 18 06.22	+22 48 05.2	2.0905	0.87	0.44	-	-	27.22	nn
J0120+2330	01 20 06.17	+23 30 39.0	0.5955	0.98	0.39	-	-	25.82	v
J0133+2427	01 33 24.63	+24 27 41.4	0.4520	0.92	0.32	-	-	26.63	v
J0133+0113	01 33 52.66	+01 13 45.2	0.3081	1.80	0.49	0.18	24.61	25.46	j
J0142+0732	01 42 39.99	+07 32 39.5	0.8960	0.69	0.32	0.05	24.98	26.37	
J0148-0819	01 48 47.61	-08 19 36.3	1.6797	0.76	0.39	0.05	25.57	27.03	
J0204-0528	02 04 06.98	-05 28 42.9	1.6160	0.90	0.46	1.39	26.71	27.07	
J0209-0808	02 09 26.41	-08 08 01.1	1.3286	1.11	0.57	-	-	26.69	
J0227-0922	02 27 40.33	-09 22 16.7	1.0150	0.55	0.27	-	-	26.60	
J0233-0012	02 33 13.82	-00 12 15.5	0.8070	0.84	0.38	0.05	25.02	26.45	
J0233-0455	02 33 22.16	-04 55 06.8	0.7800	1.12	0.50	0.73	26.22	26.67	
J0240-0450	02 40 45.79	-04 50 53.4	0.5754	1.19	0.47	0.05	24.46	25.85	
J0245+0108	02 45 34.07	+01 08 13.8	1.5310	0.96	0.49	0.03	25.84	27.54	
J0255-0259	02 55 51.48	-02 59 39.3	0.9745	1.34	0.64	0.03	25.78	27.37	

*Table 2 continued*



Table 2 (*continued*)

IAU name	$\alpha(2000)$ (h m s)	$\delta(2000)$ ( $^{\circ}$ ' ")	z	LAS <sub>FIRST</sub> (arcmin)	D <sub>FIRST</sub> (Mpc)	$f_c$	$\log P_{\text{core}}$ W Hz <sup>-1</sup>	$\log P_{\text{tot}}$ W Hz <sup>-1</sup>	Flag
(1)	(2)	(3)	(4)	(5)	(6)	(7)	(8)	(9)	(10)
J0313+0036	03 13 18.67	+00 36 23.9	1.2561	0.98	0.49	0.29	25.85	26.61	
J0341+0046	03 41 06.76	+00 46 10.1	0.6330	1.38	0.56	0.35	25.17	25.82	
J0352-0711	03 52 30.55	-07 11 02.3	0.9651	0.72	0.35	0.01	25.62	28.04	
J0726+3621	07 26 29.48	+36 21 12.9	0.9106	0.98	0.46	0.04	24.79	26.26	
J0734+3250	07 34 28.88	+32 50 58.5	1.8050	0.88	0.45	0.01	25.06	27.19	
J0741+4632	07 41 03.33	+46 32 38.0	1.1170	0.92	0.46	0.04	24.86	26.34	
J0741+3333	07 41 25.23	+33 33 20.0	0.3641	2.14	0.65	0.01	23.99	26.36	
J0742+1947	07 42 18.22	+19 47 19.5	0.6573	1.64	0.69	0.98	25.83	26.20	
J0745+3142	07 45 41.66	+31 42 56.5	0.4609	1.85	0.65	0.89	26.59	26.96	j
J0748+3328	07 48 58.31	+33 28 22.6	0.5840	1.63	0.64	0.01	24.14	26.31	
J0750+1843	07 50 44.37	+18 43 37.0	1.4900	0.44	0.22	-	-	27.20	
J0751+1152	07 51 51.55	+11 52 55.9	0.8940	0.83	0.39	-	-	26.27	j
J0752+2451	07 52 06.74	+24 51 18.8	0.8185	1.21	0.55	0.12	25.12	26.18	
J0754+4550	07 54 29.24	+45 50 50.4	1.3050	1.05	0.53	0.04	24.83	26.32	
J0801+1915	08 01 12.65	+19 15 44.8	0.4085	1.56	0.51	-	-	26.32	
J0806+4841	08 06 44.43	+48 41 49.2	0.3700	1.66	0.51	0.06	25.30	26.57	
J0807+1430	08 07 24.91	+14 30 29.4	1.2545	0.62	0.31	0.18	25.60	26.51	
J0807+4946	08 07 54.50	+49 46 27.6	0.5752	1.02	0.40	-	-	26.62	
J0809+2015	08 09 20.81	+20 15 38.5	1.1284	0.99	0.49	-	-	26.65	
J0811+4831	08 11 37.23	+48 31 33.8	0.7027	0.47	0.20	-	-	26.46	
J0812+2200	08 12 12.48	+22 00 24.3	1.1052	0.39	0.19	0.34	25.94	26.63	
J0813+5012	08 13 18.85	+50 12 39.8	0.5714	0.80	0.32	0.02	24.99	26.80	
J0815+1348	08 15 22.84	+13 48 34.1	0.8826	0.60	0.28	0.17	25.70	26.63	
J0816+1603	08 16 05.18	+16 03 45.4	1.4326	1.31	0.67	0.06	25.06	26.42	
J0817+2237	08 17 35.08	+22 37 17.7	0.9810	0.48	0.23	0.06	26.35	27.69	
J0820+5828	08 20 47.37	+58 28 45.2	0.4236	1.21	0.40	0.07	24.96	26.18	
J0821+5137	08 21 25.97	+51 37 15.5	1.4375	0.99	0.51	0.02	25.43	27.19	
J0822+0519	08 22 26.43	+05 19 51.1	0.6540	0.63	0.26	-	-	26.72	
J0823+5812	08 23 33.47	+58 12 11.1	0.7782	1.27	0.57	0.04	24.92	26.40	
J0825+4436	08 25 17.61	+44 36 26.9	0.9015	0.53	0.25	-	-	27.36	
J0828+3935	08 28 06.84	+39 35 40.3	0.7614	1.11	0.49	0.06	24.96	26.27	
J0829+1257	08 29 16.69	+12 57 15.6	1.7240	0.86	0.44	0.44	26.43	27.08	
J0831+1352	08 31 57.75	+13 52 45.9	0.6134	1.34	0.54	0.01	24.79	26.87	
J0832+1953	08 32 00.15	+19 53 12.1	1.0637	1.23	0.60	0.50	26.39	26.96	
J0834+0957	08 34 40.62	+09 57 54.9	1.7615	0.60	0.31	0.03	25.82	27.44	

Table 2 *continued*

Table 2 (*continued*)

IAU name	$\alpha(2000)$ (h m s)	$\delta(2000)$ ( $^{\circ}$ ' ")	z	LAS <sub>FIRST</sub> (arcmin)	D <sub>FIRST</sub> (Mpc)	$f_c$	$\log P_{\text{core}}$ W Hz <sup>-1</sup>	$\log P_{\text{tot}}$ W Hz <sup>-1</sup>	Flag
(1)	(2)	(3)	(4)	(5)	(6)	(7)	(8)	(9)	(10)
J0839+2928	08 39 51.75	+29 28 18.2	1.1364	0.86	0.42	0.04	25.39	26.88	
J0843+2944	08 43 09.86	+29 44 04.7	0.3978	1.41	0.45	0.02	25.00	26.68	
J0843+6129	08 43 12.42	+61 29 43.9	0.8540	0.67	0.31	-	-	27.34	
J0844+5222	08 44 24.66	+52 22 55.7	1.7088	0.94	0.48	-	-	26.88	
J0846+0704	08 46 00.34	+07 04 24.7	0.3420	1.98	0.57	0.58	25.57	26.04	
J0847+5738	08 47 46.25	+57 38 56.7	0.6610	1.04	0.44	0.07	25.25	26.52	
J0848+1420	08 48 47.74	+14 20 57.7	1.6925	0.79	0.40	0.11	26.38	27.50	
J0848+0801	08 48 56.77	+08 01 27.3	0.9580	0.45	0.21	0.18	26.03	26.92	
J0850+5437	08 50 39.96	+54 37 53.3	0.3668	2.09	0.64	0.09	24.72	25.82	j
J0851+0159	08 51 14.93	+01 59 53.2	1.0739	0.77	0.38	0.04	24.99	26.55	
J0853+4052	08 53 41.18	+40 52 21.8	0.5719	1.12	0.44	-	-	26.19	
J0857+0906	08 57 48.57	+09 06 48.1	1.6871	1.00	0.51	0.02	25.46	27.24	
J0858+4617	08 58 20.34	+46 17 22.1	0.9650	1.21	0.58	0.02	24.53	26.27	
J0859+5103	08 59 17.02	+51 03 50.0	0.9740	0.81	0.39	0.01	24.59	26.68	
J0902+4839	09 02 29.23	+48 39 06.1	1.3746	0.66	0.34	-	-	27.26	
J0904+0208	09 04 46.00	+02 08 43.0	0.7950	0.69	0.31	0.10	25.79	26.90	
J0906+0832	09 06 49.99	+08 32 55.9	1.6190	1.34	0.69	0.29	26.05	26.82	
J0910+5427	09 10 11.14	+54 27 23.6	0.6220	0.84	0.34	0.03	25.31	26.95	
J0911+1235	09 11 27.37	+12 35 46.2	0.8010	1.01	0.46	-	-	26.19	
J0912+2123	09 12 07.21	+21 23 07.9	1.2990	0.36	0.18	-	-	27.20	
J0913-0042	09 13 33.66	-00 42 50.9	0.4263	1.75	0.58	0.25	25.02	25.76	
J0915+3401	09 15 23.30	+34 01 36.4	0.9410	1.17	0.55	-	-	26.83	
J0920+1104	09 20 23.32	+11 04 19.5	1.0525	0.47	0.23	-	-	26.80	
J0921+4538	09 21 08.62	+45 38 57.4	0.1745	2.84	0.50	0.00	23.90	26.80	
J0921+3754	09 21 46.51	+37 54 08.7	1.1090	0.91	0.45	0.54	27.07	27.62	
J0924+3547	09 24 25.02	+35 47 12.7	1.3424	1.36	0.69	0.50	25.90	26.49	
J0925+1444	09 25 07.27	+14 44 25.7	0.8953	0.73	0.34	0.07	26.06	27.36	
J0926+0416	09 26 56.71	+04 16 13.2	1.0366	0.88	0.43	0.10	25.83	26.98	
J0929+5156	09 29 47.08	+51 56 55.2	0.7040	1.22	0.52	0.01	24.14	26.43	
J0931+3647	09 31 12.91	+36 47 49.3	1.3938	0.60	0.30	0.01	24.95	27.25	
J0933+4950	09 33 01.60	+49 50 29.6	0.6160	1.64	0.67	0.36	25.07	25.71	
J0933+5114	09 33 48.08	+51 14 05.3	0.5770	0.93	0.36	0.06	24.68	25.97	
J0934-0219	09 34 59.01	-02 19 09.8	0.6320	0.61	0.25	-	-	26.60	
J0935+0204	09 35 18.19	+02 04 15.5	0.6491	1.28	0.53	0.42	26.47	27.06	
J0935+0503	09 35 53.82	+05 03 53.2	1.4022	0.59	0.30	0.01	24.83	26.82	

Table 2 *continued*

Table 2 (*continued*)

IAU name	$\alpha(2000)$ (h m s)	$\delta(2000)$ ( $^{\circ}$ ' ")	z	LAS <sub>FIRST</sub> (arcmin)	D <sub>FIRST</sub> (Mpc)	$f_c$	$\log P_{\text{core}}$ W Hz <sup>-1</sup>	$\log P_{\text{tot}}$ W Hz <sup>-1</sup>	Flag
(1)	(2)	(3)	(4)	(5)	(6)	(7)	(8)	(9)	(10)
J0936+0123	09 36 28.68	+01 23 29.2	1.6655	1.11	0.57	0.10	25.22	26.39	
J0941+3853	09 41 04.00	+38 53 51.0	0.6143	0.92	0.37	-	-	26.95	
J0941+1925	09 41 15.18	+19 25 01.7	1.8720	0.41	0.21	-	-	27.11	
J0947+5154	09 47 40.01	+51 54 56.7	1.0634	1.03	0.51	0.11	25.61	26.72	j
J0952+0628	09 52 28.46	+06 28 10.5	1.3617	1.06	0.54	0.06	25.65	27.02	
J0952+0000	09 52 45.58	+00 00 15.5	1.0625	0.64	0.32	-	-	27.57	
J0954+2122	09 54 07.03	+21 22 35.9	0.2953	1.74	0.46	0.03	24.84	26.38	
J0954+3019	09 54 27.82	+30 19 13.0	0.5330	1.40	0.53	0.23	25.29	26.07	j
J1000+0005	10 00 17.68	+00 05 23.7	0.9054	0.57	0.27	0.11	26.39	27.46	
J1000+2302	10 00 56.53	+23 02 59.0	0.4816	1.79	0.64	-	-	25.35	
J1003+5253	10 03 50.71	+52 53 52.2	1.3347	0.65	0.33	0.02	25.14	26.94	
J1004+2918	10 04 03.68	+29 18 35.4	0.9043	1.39	0.65	0.03	25.14	26.73	
J1004+2225	10 04 45.75	+22 25 19.3	0.9816	1.12	0.54	0.06	26.07	27.40	
J1006+3202	10 06 27.88	+32 02 19.2	1.2765	1.26	0.64	0.04	25.10	26.65	
J1006+2701	10 06 42.62	+27 01 15.4	0.5486	1.39	0.53	0.37	25.05	25.68	
J1007+1248	10 07 26.10	+12 48 56.2	0.2406	1.86	0.42	0.01	24.38	26.28	
J1009+0529	10 09 43.56	+05 29 53.9	0.9420	1.40	0.67	0.20	25.92	26.79	
J1015+4837	10 15 57.61	+48 37 59.7	0.3853	1.84	0.58	0.01	24.10	26.36	
J1020+5209	10 20 59.86	+52 09 18.2	0.8110	1.07	0.48	0.05	24.48	25.89	
J1023+6357	10 23 13.61	+63 57 09.3	1.1944	1.34	0.67	0.14	26.00	27.02	
J1023+4824	10 23 29.79	+48 24 37.1	1.2310	0.68	0.34	-	-	27.19	
J1027+3557	10 27 47.13	+35 57 32.4	1.0030	0.99	0.48	0.12	25.19	26.26	
J1030+2756	10 30 57.52	+27 56 02.3	0.9780	0.45	0.22	-	-	27.44	
J1031+1536	10 31 25.33	+15 36 27.1	1.3473	0.95	0.48	0.51	25.81	26.40	
J1036+1211	10 36 42.98	+12 11 23.5	1.5040	0.79	0.40	0.09	25.68	26.88	
J1038+0433	10 38 42.03	+04 33 08.6	0.4232	1.37	0.46	-	-	25.73	
J1039+2632	10 39 32.16	+26 32 44.5	0.8280	0.87	0.40	0.05	25.19	26.56	
J1042+5013	10 42 07.56	+50 13 21.9	1.2729	1.16	0.58	0.00	25.22	27.78	
J1047+4919	10 47 10.97	+49 19 26.2	1.4220	0.59	0.30	0.09	26.01	27.22	
J1054+2703	10 54 26.60	+27 03 17.4	1.3991	0.76	0.39	2.37	26.60	26.87	
J1054+2526	10 54 49.54	+25 26 50.8	0.8165	0.65	0.29	0.01	24.39	26.44	
J1054-0045	10 54 57.04	-00 45 53.1	0.9169	1.12	0.53	0.01	25.03	27.32	
J1055+3726	10 55 21.24	+37 26 52.6	0.5884	1.21	0.48	0.05	24.70	26.05	
J1100+1046	11 00 47.85	+10 46 13.2	0.4220	0.63	0.21	0.67	26.16	26.60	
J1107+1628	11 07 15.04	+16 28 02.3	0.6302	0.79	0.33	0.51	26.55	27.08	

Table 2 *continued*

Table 2 (continued)

IAU name	$\alpha(2000)$ (h m s)	$\delta(2000)$ ( $^{\circ}$ ' ")	z	LAS <sub>FIRST</sub> (arcmin)	D <sub>FIRST</sub> (Mpc)	$f_c$	$\log P_{\text{core}}$ W Hz <sup>-1</sup>	$\log P_{\text{tot}}$ W Hz <sup>-1</sup>	Flag
(1)	(2)	(3)	(4)	(5)	(6)	(7)	(8)	(9)	(10)
J1107+1004	11 07 18.89	+10 04 17.7	0.6329	0.87	0.36	0.20	25.55	26.39	
J1108+6451	11 08 29.18	+64 51 32.4	0.7140	1.11	0.48	0.06	25.52	26.83	nn
J1108+3858	11 08 37.66	+38 58 42.3	0.7820	1.16	0.52	0.01	25.15	27.31	
J1110+0321	11 10 23.85	+03 21 36.2	0.9657	1.13	0.54	0.02	25.52	27.35	
J1110+3019	11 10 40.20	+30 19 09.8	1.5218	0.74	0.38	0.37	26.28	26.97	j
J1112+0120	11 12 14.45	+01 20 48.5	1.3039	0.85	0.43	0.07	25.51	26.79	
J1113+1913	11 13 37.18	+19 13 48.0	0.7830	0.85	0.38	0.02	24.31	26.15	
J1114+3043	11 14 03.43	+30 43 51.5	1.1120	1.25	0.62	0.25	25.89	26.69	
J1115+0837	11 15 25.05	+08 37 17.5	1.1510	0.83	0.41	-	-	27.01	
J1117+5758	11 17 16.61	+57 58 11.8	1.6748	0.91	0.47	0.11	25.84	26.96	j
J1118+3828	11 18 58.62	+38 28 52.2	0.7471	1.42	0.63	0.09	24.92	26.10	
J1120+2239	11 20 41.01	+22 39 02.5	1.1693	0.94	0.47	0.07	25.39	26.69	
J1122+4100	11 22 24.58	+41 00 38.9	0.7505	0.99	0.43	0.02	24.38	26.14	
J1124-0337	11 24 11.66	-03 37 04.6	0.7527	0.68	0.30	-	-	26.59	
J1126+1220	11 26 27.12	+12 20 34.8	1.1000	0.44	0.22	-	-	27.74	
J1129+3540	11 29 39.49	+35 40 20.9	0.9010	1.17	0.55	0.05	24.69	26.10	
J1129-0121	11 29 46.02	-01 21 40.6	0.7260	1.48	0.64	0.02	25.07	26.79	j
J1130+3540	11 30 02.72	+35 40 45.7	1.4840	0.71	0.37	0.06	25.68	27.04	j
J1130+2024	11 30 47.95	+20 24 04.9	1.7720	0.66	0.34	0.02	25.31	27.13	
J1131+3259	11 31 48.65	+32 59 02.2	1.2680	1.18	0.60	0.06	25.19	26.56	
J1137-0153	11 37 14.26	-01 53 34.2	1.2924	0.61	0.31	0.12	25.42	26.51	
J1140+2525	11 40 53.14	+25 25 46.5	0.2987	2.16	0.57	0.02	24.13	26.00	
J1142+2129	11 42 57.21	+21 29 11.3	1.3730	0.43	0.22	-	-	27.88	
J1148+2111	11 48 53.81	+21 11 09.8	1.0140	0.86	0.42	0.16	25.58	26.54	j
J1153+2019	11 53 07.68	+20 19 13.3	0.6799	1.46	0.62	0.06	24.48	25.80	
J1154+5620	11 54 05.37	+56 20 40.8	0.5136	0.84	0.31	0.10	25.15	26.26	
J1154+1428	11 54 36.80	+14 28 17.8	0.9678	0.93	0.45	0.14	25.27	26.25	
J1155+6539	11 55 17.88	+65 39 16.2	1.1975	1.14	0.57	-	-	27.55	nn
J1157+1902	11 57 33.49	+19 02 27.0	0.5310	0.78	0.29	0.14	25.81	26.78	
J1158+1139	11 58 25.23	+11 39 23.6	0.7510	0.92	0.41	0.04	24.06	25.54	
J1158+6254	11 58 39.90	+62 54 27.9	0.5926	1.04	0.41	0.02	25.26	27.03	
J1159+3955	11 59 36.62	+39 55 38.6	1.4480	0.61	0.31	0.02	24.97	26.85	
J1201+1809	12 01 15.49	+18 09 48.0	1.0921	1.07	0.53	0.10	25.68	26.83	
J1201+5807	12 01 23.24	+58 07 19.9	1.7803	0.72	0.37	0.01	25.30	27.56	
J1205+1514	12 05 42.42	+15 14 57.9	0.8936	1.37	0.64	0.34	25.13	25.81	

Table 2 continued

Table 2 (*continued*)

IAU name	$\alpha(2000)$ (h m s)	$\delta(2000)$ ( $^{\circ}$ ' ")	z	LAS <sub>FIRST</sub> (arcmin)	D <sub>FIRST</sub> (Mpc)	$f_c$	$\log P_{\text{core}}$ W Hz <sup>-1</sup>	$\log P_{\text{tot}}$ W Hz <sup>-1</sup>	Flag
(1)	(2)	(3)	(4)	(5)	(6)	(7)	(8)	(9)	(10)
J1209+4834	12 09 42.79	+48 34 23.3	0.7114	0.81	0.35	0.11	25.10	26.16	
J1210+3157	12 10 37.57	+31 57 06.0	0.3891	1.38	0.44	0.09	24.98	26.10	
J1211+3628	12 11 13.77	+36 28 01.1	1.3111	1.21	0.62	0.14	25.58	26.61	
J1211+1903	12 11 27.87	+19 03 25.3	0.9713	1.03	0.49	0.05	24.89	26.28	
J1211+5052	12 11 28.86	+50 52 54.3	1.3645	0.60	0.31	0.04	25.74	27.31	
J1211+6044	12 11 54.86	+60 44 26.1	0.6369	1.03	0.43	-	-	26.87	
J1212+1143	12 12 51.63	+11 43 08.6	1.3770	0.74	0.38	0.05	25.73	27.18	j
J1213+5707	12 13 40.37	+57 07 11.5	1.5815	0.88	0.45	0.10	25.39	26.58	
J1213+0001	12 13 47.53	+00 01 30.0	0.9616	1.23	0.59	0.73	26.13	26.60	
J1214+5958	12 14 27.43	+59 58 14.9	0.7140	1.34	0.58	0.08	25.66	26.86	j
J1215+0519	12 15 41.96	+05 19 32.7	0.8101	0.76	0.34	0.03	25.13	26.73	
J1217+1019	12 17 01.37	+10 19 53.0	1.8830	0.50	0.25	0.05	26.01	27.44	
J1220+0203	12 20 11.88	+02 03 42.2	0.2404	2.02	0.46	0.89	25.69	26.05	j
J1220+0928	12 20 27.99	+09 28 27.4	1.0822	0.41	0.20	-	-	27.72	
J1220-0121	12 20 45.95	-01 21 15.5	1.4554	0.92	0.47	0.47	26.37	26.98	
J1221+0755	12 21 18.52	+07 55 01.2	0.8490	1.02	0.47	0.02	24.36	26.10	
J1221+3130	12 21 53.41	+31 30 57.0	0.8275	0.73	0.33	0.05	25.96	27.33	
J1226+2020	12 26 00.03	+20 20 54.3	1.4530	1.13	0.58	0.16	26.17	27.14	j
J1226+4232	12 26 38.45	+42 32 40.1	0.9050	0.68	0.32	-	-	26.88	
J1226+0429	12 26 53.91	+04 29 19.0	0.5174	1.13	0.42	-	-	26.79	
J1227+4259	12 27 23.01	+42 59 22.0	0.9880	1.13	0.54	0.09	25.34	26.52	j
J1228+2023	12 28 11.74	+20 23 52.5	0.6997	1.42	0.61	0.02	25.58	27.38	j
J1228+3947	12 28 26.42	+39 47 54.2	1.2452	0.92	0.46	0.06	25.34	26.70	
J1230+0945	12 30 35.83	+09 45 18.9	0.6386	1.59	0.65	0.12	24.68	25.71	
J1230+3930	12 30 52.56	+39 30 00.7	2.2240	0.89	0.45	0.02	25.83	27.73	
J1234+0829	12 34 29.02	+08 29 35.4	1.0915	1.06	0.52	0.02	25.15	27.09	
J1235+2350	12 35 18.41	+23 50 13.2	1.6380	0.69	0.35	0.02	25.38	27.21	
J1236+3940	12 36 08.22	+39 40 49.4	1.2738	1.13	0.57	0.04	24.43	26.00	
J1236+0602	12 36 23.80	+06 02 08.3	1.0497	0.95	0.46	0.09	25.26	26.42	
J1236+2635	12 36 31.32	+26 35 08.7	1.3980	0.43	0.22	-	-	27.69	
J1236+2507	12 36 51.57	+25 07 50.7	0.5447	1.43	0.55	0.08	25.22	26.43	
J1237+6634	12 37 04.76	+66 34 54.5	0.8521	0.81	0.37	-	-	26.96	v
J1237+2458	12 37 14.03	+24 58 05.0	1.3261	0.45	0.23	-	-	27.49	
J1237+3614	12 37 40.57	+36 14 01.6	1.7794	0.52	0.27	0.03	25.84	27.50	
J1238+4124	12 38 19.63	+41 24 20.5	0.4987	1.45	0.53	0.21	24.77	25.59	

Table 2 *continued*

Table 2 (continued)

IAU name	$\alpha(2000)$ (h m s)	$\delta(2000)$ ( $^{\circ}$ ' ")	z	LAS <sub>FIRST</sub> (arcmin)	D <sub>FIRST</sub> (Mpc)	$f_c$	$\log P_{\text{core}}$ W Hz <sup>-1</sup>	$\log P_{\text{tot}}$ W Hz <sup>-1</sup>	Flag
(1)	(2)	(3)	(4)	(5)	(6)	(7)	(8)	(9)	(10)
J1238+1745	12 38 35.50	+17 45 44.7	0.5175	1.78	0.66	0.04	23.85	25.38	
J1239+1954	12 39 44.96	+19 54 25.5	0.2397	2.67	0.60	0.02	23.48	25.28	fn
J1239+1800	12 39 59.78	+18 00 57.7	1.2763	1.00	0.50	0.07	25.73	27.02	j
J1240+0340	12 40 00.93	+03 40 51.8	1.8819	0.96	0.49	0.11	25.93	27.08	
J1240+3303	12 40 44.68	+33 03 49.9	0.8120	0.65	0.29	0.03	25.12	26.73	
J1241+5141	12 41 16.49	+51 41 30.0	0.8231	1.06	0.48	0.11	25.73	26.83	
J1241+4523	12 41 32.88	+45 23 12.1	0.7353	1.34	0.58	0.02	24.58	26.29	j
J1241+4934	12 41 39.72	+49 34 05.5	0.4738	0.92	0.33	0.06	24.72	26.00	
J1242+4356	12 42 19.25	+43 56 08.2	0.6123	0.88	0.36	-	-	26.81	
J1243+6155	12 43 08.34	+61 55 08.2	1.6513	0.51	0.26	0.04	25.77	27.33	
J1246+3452	12 46 41.90	+34 52 51.3	1.0262	0.91	0.44	0.06	25.55	26.86	
J1249+4444	12 49 23.51	+44 44 50.4	0.8030	0.46	0.21	-	-	27.22	
J1251+4918	12 51 51.03	+49 18 55.1	1.4626	0.66	0.34	0.12	26.09	27.18	
J1253+2627	12 53 02.25	+26 27 22.5	1.2575	0.91	0.46	0.01	24.89	27.14	
J1255+4809	12 55 03.88	+48 09 53.0	1.7050	0.50	0.25	0.13	26.50	27.56	
J1255+2714	12 55 20.63	+27 14 09.3	1.7390	0.88	0.45	0.11	25.38	26.50	
J1259+6523	12 59 48.77	+65 23 44.4	1.0308	1.16	0.56	-	-	26.39	nn
J1300+1526	13 00 44.66	+15 26 20.5	1.4920	0.61	0.31	0.24	26.06	26.89	
J1307+0922	13 07 30.02	+09 22 05.2	0.2586	2.63	0.63	0.08	23.78	24.95	
J1308-0128	13 08 12.02	-01 28 59.9	1.0190	0.76	0.37	0.03	25.66	27.34	j
J1309+0828	13 09 36.24	+08 28 15.3	0.7780	1.02	0.46	0.03	24.89	26.51	
J1311+3942	13 11 33.02	+39 42 57.7	0.6290	1.27	0.52	0.30	25.15	25.85	
J1311+2008	13 11 54.52	+20 08 54.1	1.2900	0.69	0.35	0.03	24.81	26.42	
J1314+0911	13 14 59.36	+09 11 36.6	0.8230	1.09	0.50	0.16	25.15	26.09	
J1321+6215	13 21 27.57	+62 15 32.2	0.8980	1.15	0.54	0.01	24.49	26.72	
J1322+0825	13 22 03.30	+08 25 54.3	1.8890	0.86	0.44	0.12	26.05	27.18	
J1322+1848	13 22 20.15	+18 48 26.4	1.5550	1.17	0.60	0.07	25.93	27.23	
J1326+4737	13 26 31.45	+47 37 55.9	0.6821	0.88	0.37	0.20	25.33	26.18	
J1326+2131	13 26 54.71	+21 31 26.1	1.1013	1.25	0.62	0.12	25.96	27.02	
J1327+4842	13 27 46.16	+48 42 03.0	1.0304	0.75	0.37	0.14	25.64	26.64	
J1330+6237	13 30 57.58	+62 37 22.4	0.9540	1.38	0.66	0.02	24.67	26.50	
J1331+3756	13 31 26.35	+37 56 04.9	1.0527	1.23	0.60	0.06	25.40	26.73	
J1332+0200	13 32 53.27	+02 00 45.7	0.2158	1.99	0.41	0.16	25.64	26.52	
J1334+4511	13 34 33.52	+45 11 42.1	0.7394	1.10	0.48	0.46	25.68	26.26	
J1334+3128	13 34 49.73	+31 28 24.1	1.3093	0.83	0.42	0.90	26.13	26.56	

Table 2 continued

Table 2 (*continued*)

IAU name	$\alpha(2000)$ (h m s)	$\delta(2000)$ ( $^{\circ}$ ' ")	z	LAS <sub>FIRST</sub> (arcmin)	D <sub>FIRST</sub> (Mpc)	$f_c$	$\log P_{\text{core}}$ W Hz <sup>-1</sup>	$\log P_{\text{tot}}$ W Hz <sup>-1</sup>	Flag
(1)	(2)	(3)	(4)	(5)	(6)	(7)	(8)	(9)	(10)
J1336+6541	13 36 55.51	+65 41 16.0	0.4375	1.19	0.40	-	-	26.08	v
J1341+1556	13 41 14.38	+15 56 35.2	1.7100	0.70	0.36	0.01	25.14	27.27	
J1342+2828	13 42 54.38	+28 28 05.9	1.0353	0.57	0.28	0.61	26.38	26.90	
J1345+4125	13 45 23.83	+41 25 41.6	0.9165	0.89	0.42	0.50	25.72	26.28	
J1347+6221	13 47 39.84	+62 21 49.5	0.8038	1.43	0.65	0.03	24.60	26.15	j
J1350+1645	13 50 31.51	+16 45 24.1	1.9316	1.16	0.59	0.70	26.23	26.76	
J1350+0522	13 50 54.59	+05 22 06.4	0.4421	1.11	0.38	0.23	25.24	26.01	
J1351+4106	13 51 55.75	+41 06 31.7	0.7643	0.81	0.36	0.03	24.51	26.06	
J1357+2047	13 57 07.19	+20 47 42.0	0.5443	1.76	0.67	0.07	24.44	25.68	
J1359+0159	13 59 27.15	+01 59 54.6	1.3290	0.73	0.37	44.0	27.72	27.84	
J1402+5204	14 02 27.28	+52 04 32.2	0.8730	0.60	0.28	-	-	26.88	
J1402+2112	14 02 46.83	+21 12 48.0	0.7529	0.87	0.38	0.20	24.83	25.68	
J1405+2925	14 05 00.81	+29 25 14.1	0.6970	1.15	0.49	0.03	25.07	26.66	j
J1406+2509	14 06 26.60	+25 09 21.1	0.8670	1.40	0.65	0.71	26.27	26.73	
J1408+0031	14 08 32.65	+00 31 38.6	1.6723	0.93	0.48	0.02	25.09	26.90	
J1410+2649	14 10 22.28	+26 49 25.3	1.8610	0.96	0.49	0.13	25.45	26.54	
J1411+1953	14 11 08.04	+19 53 03.2	0.5199	0.51	0.19	-	-	25.83	
J1411+0659	14 11 18.29	+06 59 06.3	1.8120	0.79	0.40	0.04	25.49	27.08	
J1412+5455	14 12 31.18	+54 55 11.5	1.5233	0.49	0.25	0.09	26.01	27.22	
J1416+3447	14 16 17.06	+34 47 44.7	2.9020	0.74	0.35	0.07	26.42	27.79	
J1417+2317	14 17 17.90	+23 17 20.2	0.9215	0.55	0.26	0.38	26.16	26.81	
J1418+1921	14 18 23.28	+19 21 57.1	1.0257	0.89	0.43	0.08	25.47	26.69	
J1418+1107	14 18 59.39	+11 07 17.3	0.5630	1.73	0.67	0.05	24.32	25.71	
J1426+4024	14 26 06.19	+40 24 32.0	0.6638	1.40	0.59	0.22	25.55	26.36	
J1427+3247	14 27 58.73	+32 47 41.5	0.5695	1.49	0.58	0.15	25.24	26.19	
J1430+0823	14 30 59.00	+08 23 42.0	0.6269	0.88	0.36	0.08	25.51	26.70	
J1431+0638	14 31 45.04	+06 38 09.2	0.6700	0.75	0.31	0.30	25.52	26.23	
J1432-0059	14 32 44.44	-00 59 15.1	1.0264	0.69	0.34	0.15	25.76	26.75	
J1434-0123	14 34 10.77	-01 23 41.7	1.0204	1.00	0.49	0.03	25.12	26.74	
J1436+6428	14 36 08.72	+64 28 04.0	0.5914	1.13	0.45	0.02	24.15	26.04	
J1436+0618	14 36 23.66	+06 18 48.7	0.9655	0.68	0.33	0.06	25.13	26.47	
J1443+3154	14 43 17.59	+31 54 56.8	0.9709	0.48	0.23	0.06	25.20	26.57	
J1443+0809	14 43 25.32	+08 09 57.4	0.7808	0.87	0.39	0.59	25.62	26.12	
J1444+4107	14 44 35.11	+41 07 07.9	0.6630	0.94	0.40	0.03	24.58	26.21	
J1446+1222	14 46 00.03	+12 22 40.5	0.5134	1.47	0.54	0.06	25.21	26.54	

Table 2 *continued*



Table 2 (continued)

IAU name	$\alpha(2000)$ (h m s)	$\delta(2000)$ ( $^{\circ}$ ' ")	z	LAS <sub>FIRST</sub> (arcmin)	D <sub>FIRST</sub> (Mpc)	$f_c$	$\log P_{\text{core}}$ W Hz <sup>-1</sup>	$\log P_{\text{tot}}$ W Hz <sup>-1</sup>	Flag
(1)	(2)	(3)	(4)	(5)	(6)	(7)	(8)	(9)	(10)
J1446+0046	14 46 36.90	+00 46 56.6	0.7231	0.79	0.34	0.20	25.36	26.20	
J1448+4352	14 48 31.80	+43 52 33.0	0.7840	0.96	0.43	0.01	24.90	27.08	
J1449+3948	14 49 29.62	+39 48 24.3	1.4910	0.73	0.37	0.08	26.25	27.51	
J1449+4519	14 49 45.04	+45 19 41.3	1.6339	1.11	0.57	3.04	26.54	26.79	
J1451+0159	14 51 34.61	+01 59 37.0	1.2745	1.04	0.53	0.16	25.48	26.45	
J1452+4522	14 52 24.67	+45 22 23.7	0.4682	1.34	0.47	0.23	25.66	26.44	
J1453+0934	14 53 53.90	+09 34 23.2	0.6273	0.49	0.20	0.30	26.20	26.90	
J1500+4508	15 00 27.22	+45 08 59.1	1.2032	0.79	0.40	0.11	25.83	26.93	
J1500+5227	15 00 58.51	+52 27 10.3	0.8370	0.65	0.30	-	-	26.55	
J1511-0047	15 11 19.52	-00 47 37.8	0.6600	1.28	0.53	0.01	24.52	26.44	
J1511+1015	15 11 22.01	+10 15 35.0	0.7663	1.01	0.45	0.06	25.21	26.54	
J1511+3228	15 11 30.79	+32 28 21.1	0.6530	1.11	0.46	0.09	25.28	26.44	
J1511+4430	15 11 42.77	+44 30 43.6	0.9652	0.49	0.24	-	-	27.22	
J1513+1011	15 13 29.29	+10 11 05.6	1.5470	0.59	0.30	0.15	26.37	27.38	
J1514+3650	15 14 43.07	+36 50 50.4	0.3710	0.94	0.29	0.08	25.44	26.60	
J1517+4351	15 17 45.77	+43 51 04.9	1.9050	1.12	0.57	0.02	25.57	27.47	
J1519+3749	15 19 12.82	+37 49 18.4	2.1600	0.82	0.41	0.06	25.73	27.15	
J1519+1415	15 19 15.77	+14 15 02.5	1.8200	1.09	0.56	0.37	26.06	26.77	
J1519+3844	15 19 32.08	+38 44 52.6	1.5200	0.61	0.31	1.20	26.64	27.02	
J1524+0828	15 24 59.50	+08 28 51.9	1.0137	0.91	0.44	0.03	24.97	26.60	
J1528+5637	15 28 06.08	+56 37 06.4	1.2180	1.19	0.60	0.18	25.64	26.57	
J1528+4847	15 28 38.40	+48 47 40.6	1.0270	1.22	0.59	0.03	24.96	26.53	
J1531+5844	15 31 07.40	+58 44 09.9	1.7210	1.31	0.67	0.07	26.27	27.60	
J1531+0338	15 31 28.69	+03 38 02.3	0.7530	1.23	0.54	0.45	25.86	26.45	
J1532+4954	15 32 46.69	+49 54 58.5	0.5442	1.34	0.51	0.13	24.32	25.33	
J1532+1022	15 32 56.28	+10 22 39.3	0.6378	0.97	0.40	0.31	25.16	25.85	
J1534+5045	15 34 09.80	+50 45 12.9	0.8100	1.13	0.51	0.17	25.00	25.92	
J1541+0050	15 41 12.88	+00 50 32.1	1.1387	0.91	0.45	0.03	25.97	27.64	
J1542+1054	15 42 56.12	+10 54 36.5	0.9930	0.61	0.29	0.13	26.05	27.08	
J1543+1021	15 43 18.85	+10 21 44.3	1.0420	0.82	0.40	0.03	24.88	26.46	
J1546+3644	15 46 38.31	+36 44 20.2	0.9393	0.90	0.43	0.86	26.13	26.55	
J1550+3652	15 50 02.01	+36 52 16.7	2.0790	1.35	0.69	0.03	25.37	26.99	
J1550+2539	15 50 04.46	+25 39 37.9	1.5506	0.71	0.36	0.18	26.03	26.96	
J1550+0744	15 50 22.30	+07 44 53.7	1.0524	1.03	0.50	0.04	25.21	26.76	
J1550+1120	15 50 43.59	+11 20 47.5	0.4357	0.81	0.27	0.34	26.05	26.69	

Table 2 continued

Table 2 (*continued*)

IAU name	$\alpha(2000)$ (h m s)	$\delta(2000)$ ( $^{\circ}$ ' ")	z	LAS <sub>FIRST</sub> (arcmin)	D <sub>FIRST</sub> (Mpc)	$f_c$	$\log P_{\text{core}}$ W Hz <sup>-1</sup>	$\log P_{\text{tot}}$ W Hz <sup>-1</sup>	Flag
(1)	(2)	(3)	(4)	(5)	(6)	(7)	(8)	(9)	(10)
J1551+4810	15 51 27.31	+48 10 50.8	0.7040	0.86	0.37	0.08	24.76	25.96	
J1553+1400	15 53 06.19	+14 00 58.6	0.8170	1.25	0.57	0.07	25.64	26.89	
J1556+0405	15 56 23.17	+04 05 20.2	1.4870	0.75	0.39	-	-	26.64	
J1557+3304	15 57 29.94	+33 04 46.9	0.9496	0.57	0.27	1.08	26.41	26.78	
J1601+3026	16 01 26.43	+30 26 58.8	0.8490	0.55	0.25	0.07	24.92	26.19	
J1609+6109	16 09 02.41	+61 09 44.8	0.9040	1.22	0.57	-	-	26.34	
J1609+0611	16 09 24.45	+06 11 29.2	0.7870	0.65	0.29	-	-	26.74	
J1613+2123	16 13 41.97	+21 23 07.2	0.9267	1.21	0.57	0.12	25.01	26.08	
J1613+3907	16 13 42.98	+39 07 32.9	0.9762	0.87	0.42	0.06	25.85	27.22	
J1617+1435	16 17 42.85	+14 35 53.6	0.6572	1.42	0.59	0.06	24.48	25.77	
J1620+1736	16 20 21.82	+17 36 23.9	0.5551	0.85	0.33	0.14	26.34	27.31	
J1620+2939	16 20 42.20	+29 39 07.2	1.3450	0.95	0.48	0.01	25.46	27.51	
J1620+4217	16 20 43.40	+42 17 18.9	1.0480	0.71	0.35	0.01	24.98	27.07	
J1620+4900	16 20 56.63	+49 00 03.6	1.4490	0.78	0.40	0.12	25.33	26.42	
J1622+2900	16 22 46.27	+29 00 54.2	2.1484	0.98	0.49	0.10	25.52	26.74	
J1624+2345	16 24 39.09	+23 45 12.2	0.9274	0.44	0.21	-	-	27.94	
J1628+4552	16 28 51.27	+45 52 18.6	0.6753	0.80	0.34	-	-	26.33	
J1629+4434	16 29 17.79	+44 34 52.5	1.0340	1.00	0.48	0.09	25.05	26.24	
J1631+3023	16 31 37.53	+30 23 41.3	1.2608	1.29	0.65	0.36	25.89	26.58	
J1635+3110	16 35 24.18	+31 10 00.6	1.1305	0.91	0.45	0.01	24.65	26.65	
J1637+4130	16 37 02.21	+41 30 22.2	1.1786	1.04	0.52	-	-	27.09	
J1640+1936	16 40 13.40	+19 36 20.3	0.7750	0.53	0.24	0.53	25.86	26.39	
J1652+4900	16 52 50.46	+49 00 38.8	1.5713	1.20	0.61	0.07	24.89	26.19	
J1654+1847	16 54 38.44	+18 47 45.3	1.3600	0.67	0.34	0.04	25.41	26.90	
J1657+2813	16 57 39.38	+28 13 29.3	1.0882	1.17	0.58	0.21	24.99	25.85	
J1658+6238	16 58 19.52	+62 38 23.1	0.7032	1.08	0.46	0.06	24.46	25.77	
J1658+2254	16 58 55.73	+22 54 20.0	0.5242	1.56	0.59	0.01	23.86	25.79	
J1702+5915	17 02 20.06	+59 15 38.6	1.7984	0.80	0.41	0.03	26.04	27.74	j
J1704+3854	17 04 04.50	+38 54 30.8	0.8815	0.54	0.25	0.02	24.91	26.75	
J1704+4247	17 04 52.44	+42 47 58.2	0.6670	1.52	0.64	-	-	25.18	fn
J1706+3214	17 06 48.06	+32 14 22.9	1.0698	0.91	0.45	0.67	26.31	26.80	j
J1707+3345	17 07 26.32	+33 45 13.5	0.6310	0.54	0.22	0.28	25.16	25.89	
J1708+2435	17 08 46.13	+24 35 28.9	1.3577	0.77	0.39	0.07	26.18	27.48	
J1715+2844	17 15 54.63	+28 44 49.9	1.4586	0.68	0.35	0.15	25.39	26.39	
J2039-0024	20 39 52.17	-00 24 47.1	0.6130	1.26	0.51	0.44	25.41	25.98	

Table 2 *continued*

Table 2 (*continued*)

IAU name	$\alpha(2000)$ (h m s)	$\delta(2000)$ ( $^{\circ}$ ' ")	z	LAS <sub>FIRST</sub> (arcmin)	D <sub>FIRST</sub> (Mpc)	$f_c$	$\log P_{\text{core}}$ W Hz <sup>-1</sup>	$\log P_{\text{tot}}$ W Hz <sup>-1</sup>	Flag
(1)	(2)	(3)	(4)	(5)	(6)	(7)	(8)	(9)	(10)
J2130-0102	21 30 04.76	-01 02 44.5	0.7040	0.53	0.23	-	-	26.85	
J2141-0639	21 41 11.90	-06 39 30.3	0.5518	1.20	0.46	0.13	24.65	25.63	
J2212+2250	22 12 06.93	+22 50 37.1	0.8820	1.26	0.59	-	-	26.23	v
J2214+0052	22 14 09.96	+00 52 27.0	0.9078	0.69	0.32	0.25	25.84	26.62	
J2220-0022	22 20 30.09	-00 22 16.3	0.6023	1.56	0.63	-	-	26.19	
J2221+1429	22 21 36.79	+14 29 56.4	2.2770	0.41	0.21	0.10	26.31	27.50	
J2227+0005	22 27 29.06	+00 05 21.9	1.5133	0.34	0.17	1.32	26.90	27.27	
J2232+2229	22 32 05.82	+22 29 17.8	0.6590	0.96	0.40	-	-	25.93	v
J2241+1837	22 41 27.88	+18 37 36.5	0.9492	0.94	0.45	-	-	26.60	v
J2247+1246	22 47 25.64	+12 46 24.8	0.6860	1.43	0.61	-	-	26.07	
J2256+3038	22 56 10.04	+30 38 05.2	0.8430	0.74	0.34	-	-	26.56	v
J2302-0320	23 02 36.14	-03 20 21.0	0.8480	1.31	0.60	-	-	25.76	
J2308+2410	23 08 39.54	+24 10 27.7	1.2474	0.91	0.46	-	-	26.47	nn
J2315+2154	23 15 59.00	+21 54 29.3	1.1705	0.63	0.32	-	-	26.94	v
J2322+2113	23 22 02.61	+21 13 56.5	0.7079	1.30	0.56	-	-	26.44	nn
J2335-0052	23 35 15.42	-00 52 21.7	1.2900	0.53	0.27	0.04	25.16	26.74	
J2336+0002	23 36 24.05	+00 02 46.0	1.0949	1.03	0.51	0.09	25.90	27.09	j
J2339+1038	23 39 39.77	+10 38 42.7	0.7730	1.16	0.52	0.02	23.96	25.83	
J2340+1923	23 40 23.75	+19 23 22.7	0.8720	0.93	0.43	-	-	26.28	v
J2345-0936	23 45 40.44	-09 36 10.2	1.2754	1.05	0.53	0.04	25.69	27.20	j
J2359+0206	23 59 15.66	+02 06 54.6	0.5700	0.69	0.27	-	-	26.47	